# On climate and abyssal circulation in the Atlantic Ocean during late Pliocene marine isotope stage M2, ~3.3 million years ago

**Nicola Kirby[1,2], Ian Bailey*[3], David C. Lang[1], Anieke Brombacher[1], Thomas B. Chalk[1], Rebecca L. Parker[3], Anya J. Crocker[1], Victoria E. Taylor[1], James A. Milton[1], Gavin L. Foster[1], Maureen E. Raymo[4], Dick Kroon[5], David B. Bell[5], Paul A. Wilson[1]**

1. School of Ocean and Earth Science, University of Southampton, Waterfront Campus, National Oceanography Centre Southampton, European Way, Southampton SO14 3ZH, UK.

2. Now at: Earth Sciences, School of Geography, Earth and Environmental Sciences, University of Birmingham B15 2TT, UK.

3. Camborne School of Mines, College of Engineering, Mathematics & Physical Sciences, University of Exeter, Penryn Campus, Treliever Road, Penryn TR10 9FE, UK.

4. Columbia University, Lamont-Doherty Earth Observatory, P.O. Box 1000, 61 Route 9W, Palisades, NY 10964, USA.

5. School of GeoSciences, University of Edinburgh, Edinburgh EH9 3JW, UK

6. Centre for Environmental Policy, Weeks Building, 16-18 Prince's Gardens, Imperial College London South Kensington, London SW7 1NE, UK.

*corresponding author: njk883@student.bham.ac.uk

**Abstract:** Marine Isotope Stage (MIS) M2, 3.3 Ma, is an isolated cold stage punctuating the benthic oxygen isotope ($\delta^{18}O$) stratigraphy of the warm Piacenzian interval of the late Pliocene Epoch. The prominent (~0.65‰) $\delta^{18}O$ increase that defines MIS M2 has prompted debate over the extent to which it signals an early

prelude to the rhythmic extensive glaciations of the northern hemisphere that

characterise the Quaternary and raised questions about the forcing mechanisms

responsible. Recent work suggests that $CO_2$ storage in the deep Atlantic Ocean played

an important role in these events but detailed reconstructions of deep ocean chemical

stratification are needed to test this idea and competing hypotheses. Here we present

new records of the Nd isotope composition of fish debris and $\delta^{13}C$ and B/Ca ratios of

benthic foraminifera from the northwest and southeast Atlantic Ocean. Our novel

geochemical data show that, in contrast to major Quaternary glaciations such as MIS

2 (~21 kyr) and MIS 100 (~2.52 Ma), the deep North Atlantic Ocean was weakly

chemically stratified during MIS M2. We show that Southern Component Water

incursion into the Atlantic Ocean was limited to the deep South Atlantic basin during

MIS M2 and peaked well before (~10-15-kyr) the atmospheric $CO_2$ minimum. Our

findings imply that the deep Atlantic Ocean was not the principle sink of $CO_2$

sequestered from the atmosphere during MIS M2, implicating a different $CO_2$ storage

deep-water reservoir mechanism, presumably Southern Component Water incursion

into the Pacific Ocean. Weak chemical stratification in the deep Atlantic Ocean

during MIS M2 relative to MIS 100 and 2 suggests comparatively active Atlantic

meridional overturning circulation. That suggestion is consistent with the warmth of

the high latitude North Atlantic during MIS M2 – surface water temperatures cooled

during M2 but only to Holocene values. Our findings may help to explain the paucity

of evidence for extensive early glaciation of the northern hemisphere during M2 but

leave open the possibility of ice sheet advance on Antarctica.

52

## 1. Introduction

Much of the Pliocene Epoch is considered to have been warmer than the pre-industrial with peak atmospheric carbon dioxide ($pCO_2$) levels about as high as present (413 ppm in 2019; Seki et al., 2010; Dowsett et al., 2012; Haywood et al., 2013; Martinez-Boti et al., 2015; de la Vega et al., 2020). Many studies of Pliocene warmth over the past two decades have focused on the mid-Piacenzian warm period (mPWP, 3.264 to 3.025 Ma), the most recent interval of sustained warmth during this epoch (McClymont et al., 2020). However, just prior to this time there occurred a transient interval of high latitude cooling beginning around 3.5 Ma during Marine Isotope Stage (MIS) MG5 that culminated during MIS M2, 3.295 Ma (Prell, 1984; Keigwin, 1987; Haug and Tiedemann, 1998; Jansen et al., 2000; Lisiecki and Raymo, 2005).

One interpretation of MIS M2 is that it signals early extensive northern hemisphere (and therefore) bi-polar glaciation (De Schepper et al, 2009; De Schepper et al., 2013). Yet the magnitude and location of land ice growth during this cold stage is poorly documented – if there was a major glacial advance it is not even known whether it was concentrated in the northern or southern hemisphere (e.g., Prell, 1984; Maslin et al., 1998; Dwyer and Chandler, 2009; De Schepper et al., 2009; Naish et al., 2009; McKay et al., 2012; Gao et al., 2012; De Schepper et al., 2013; De Schepper et al., 2014; Brigham-Grette et al., 2013; Dolan et al., 2015). Estimates of global sea-level fall associated with full glacial conditions of MIS M2 range from ~ 10 m lower than the present day (Naish et al., 1997; Miller et al., 2012) to as much as 65 m lower (Dwyer and Chandler, 2009). If the larger sea-level fall estimates relative to modern are substantiated, MIS M2 may mark the first time during the Cenozoic when the seawater component of benthic $\delta^{18}O$ increase was controlled by ice sheet growth in

the northern hemisphere. Yet while there is firm evidence for glacial expansion on

Greenland, Svalbard and Iceland during M2, the same is not true of North America or

mainland Eurasia (De Schepper et al., 2014). Furthermore, numerical ice-sheet

modelling experiments, simulate only small ice caps in the northern hemisphere,

equivalent to ~12 m fall in sea level (msle) (Tan et al., 2017), twice the seawater

equivalent of the modern Greenland Ice Sheet but an order of magnitude smaller than

the fall associated with the major glaciation of the Last Glacial Maximum (Lambeck

et al., 2014).

A small M2 ice-sheet budget for the northern hemisphere is also implied by a

new detailed record of atmospheric $CO_2$ for late Pliocene which shows a marked

decline during MIS M2 (from ~420 to 310 ppm) but to concentrations unlikely to

have fallen below the threshold suggested (DeConto et al., 2008) to trigger extensive

northern hemisphere glaciation (de la Vega et al., 2020). Atmospheric $CO_2$ decline

during MIS M2 lags benthic $\delta^{18}O$ by ~10 kyr but is in-phase with possible evidence

for Southern Component Water (SCW) incursion into the deep mid-latitude North

Atlantic Ocean (Lang et al., 2016; de la Vega et al., 2020). These observations imply

that expansion of a $CO_2$-charged SCW reservoir in the deep Atlantic may have been

active more than 600-kyr before the onset of significant northern hemisphere

glaciation ~2.72 Ma (de la Vega et al., 2020). Yet, while Nd isotope and $\delta^{13}C$ records

from Integrated Ocean Drilling Program (IODP) Site U1313 (Fig. 1) suggest that

major incursions of SCW of last glacial-magnitude occurred at this site during large

Quaternary glacials at least from MIS 100, 2.52 Ma (Lang et al., 2014; 2016), those

records are insufficiently resolved for MIS M2 to provide a clear test of whether the

same is true for this older more enigmatic cold stage (Fig. 1a,b).

To shed new light on the role of the Atlantic Ocean in $CO_2$ decline during MIS

102   M2, we present a new high-resolution (suborbital-scale) assessment of changes in

103   water-mass distribution at deep Northwest Atlantic Ocean IODP Site U1313 (Fig. 2)

104   and deep Southeast Atlantic Ocean Drilling Program (ODP) Site 1267 (~4350 m

105   depth; ~29°S, Fig. 2). We apply the same multi-proxy approach shown to be effective

106   for tracking water-mass distribution during the last glacial (e.g., Yu et al., 2008; Chalk

107   et al., 2019), combining neodymium-isotope composition of fish debris as well as the

108   carbon isotope and B/Ca composition of benthic foraminifera to trace water-mass

109   properties. Our new records for MIS M2 show contrasting structure to that seen for

110   MIS 100 and MIS 2, strongly suggesting that the water-mass structure of the deep

111   Atlantic Ocean during MIS M2 was quite different to that of large Quaternary

112   glacials. We compare our data to published records for MIS M2 and discuss the

113   implications of our new findings for our understanding of late Pliocene climate.

114

115   **2. Methods**

116   2.1. Study sites, sampling and chronology

117   We document change in three water-mass tracers ($\delta^{13}$C and B/Ca in benthic

118   foraminiferal calcite and Nd isotopes in fish debris) for MIS M2 from the deep

119   western North Atlantic (Site U1313; Fig. 2) and deep eastern South Atlantic (Site

120   1267; Fig. 2) and compare their amplitude of change to new and published records for

121   MIS 100 (2.52 Ma) and MIS 2 (21 ka), large Quaternary glacials for which major

122   SCW incursion into the deep North Atlantic is documented by characteristic $\delta^{13}$C-

123   $CO_3^{2-}$-Nd isotope relationships (e.g., Oppo and Fairbanks, 1987; Raymo et al., 1987,

124   1990, 1992; Hodell and Venz, 1992; Yu et al., 2008; Lang et al., 2016; Chalk et al.,

125   2019). Given the caveats that come with water-mass provenance proxies, we follow

126   Lang et al. (2016) in placing most confidence in signals of change documented in all

127    three water-mass-proxy records. To produce our new data sets we: 1) increased the

128    resolution of the Site U1313 fish debris Nd isotope record published by Lang et al.

129    (2016) for MIS M2 and MIS 100 (from ~6-7 kyr to ~3.5 and 1 kyr, respectively), and

130    2) developed new suborbitally resolved records of fish debris Nd isotopes and benthic

131    foraminiferal B/Ca ratios and $\delta^{13}C$ for MIS M2 (3.24-3.33 Ma), 100 (2.5-2.55 Ma)

132    and the last glacial-Holocene (0-40 ka) from Site 1267.

133

134    2.1.1. IODP Site U1313

135    IODP Site U1313 (41˚N, 32.4˚W, 3426 m depth, Fig. 2) constitutes a re-occupation of

136    Deep Sea Drilling Project (DSDP) Site 607, a benchmark site for monitoring North

137    Atlantic Deep Water (NADW) production during the Plio-Pleistocene (e.g.,

138    Ruddiman et al., 1989; Raymo et al., 1990, 1992; Raymo et al., 2004). Today, Site

139    U1313 is bathed by 100% lower NADW. To increase the resolution of the previously

140    published fish debris Nd isotope record for Site U1313 spanning MIS M2 and MIS

141    100, we analysed 14 additional samples from the shipboard primary splice (between

142    152.48-154.38 mcd; Expedition 306 Scientists, 2006) and 42 samples from the

143    shipboard secondary splice (between 118.74-121.39 mcd; Expedition 306 Scientists,

144    2006). The age model for our MIS M2 record is based on retuning the Site U1313

145    benthic $\delta^{18}O$ stratigraphy (Bolton et al., 2010) to the LR04 stack (Lisiecki and

146    Raymo, 2005) (Supplementary Information Section S2). To improve the age model

147    for the Site U1313 stratigraphy spanning MIS 100 (which was previously based on

148    assigning ages from the primary splice to the secondary splice stratigraphy by

149    correlating between the two using shipboard-derived sediment colour reflectance data;

150    Lang et al., 2016), we generated a new suborbitally resolved benthic foraminiferal

151    $\delta^{18}O$ record (at on average ~1 kyr) between 118.64-122.44 mcd from the secondary

152    splice, which we subsequently tuned to the LR04 stack (Supplementary Information

153    Section S2).

154

155    2.1.2. ODP Site 1267

156    ODP Site 1267 (29˚S, 2˚E at 4350 m depth; Fig. 2) sits in the Angola Basin in the

157    Southeast Atlantic and monitors bottom-water conditions at the base of the northern

158    face of Walvis Ridge. Today Site 1267 is bathed by Lower Deep Water (LDW), a

159    mixture of 70-80% North Atlantic Deep Water (NADW) and 20-30% Antarctic

160    Bottom Water (AABW) sourced from the western Atlantic via the equatorial

161    Romanche and Chain Fracture zones and mixed vertically in the Angola Basin

162    downstream of these entry points (Fig. 2; Mercier and Morin, 1997; Arhan et al.,

163    2003). The Rio de Janeiro and Rio Grande Fracture zones, which cut the Mid-

164    Atlantic Ridge at 4000 m or greater depth at 21˚S and 26˚S, respectively, also funnel

165    AABW from the western South Atlantic Brazil Basin into the Angola Basin (Fig. 2;

166    Mercier et al., 2000). Together with two other passages below 4000 m in the southern

167    part of the Walvis Ridge near 36˚S 7˚W (the Walvis Passage) and 30˚S 2˚W (Connary

168    and Ewing, 1974), these fracture zones are the only pathways for AABW to reach Site

169    1267 (Fig. 2). During late Pleistocene glacials this site was more influenced by

170    AABW (with its relatively low $\delta^{13}$C, radiogenic Nd isotope and low carbonate ion

171    signature) because the interface between AABW and overlying NADW shoaled and

172    moved equatorward allowing more southern source deep water to enter the basin via

173    these fracture zones (Yu et al., 2008; Chalk et al., 2019; Farmer et al., 2019;

174    Pöppelmeier et al., 2020). The more southerly location (by ~70˚ of latitude) and

175    greater depth (by ~900 m) of Site 1267 relative to Site U1313 allows us to investigate

176  changes in the extent of SCW incursion northwards and shoaling of its interface with

177  Northern Component Water (NCW) during MIS 2, 100 and M2.

178      To develop new records of Nd isotopes from fish debris and benthic

179  foraminiferal B/Ca ratios from Site 1267 for MIS M2, MIS 100 and the last glacial-

180  Holocene we analysed 89 samples taken from the shipboard primary splice between

181  0-0.34 mcd, 29.4-29.95 mcd and 40.27-41.42 mcd (41 of which were originally used

182  to generate the published benthic $\delta^{18}O$ and $\delta^{13}C$ stratigraphies for Site 1267; Bell et

183  al., 2014). The published age model for this site is based on alignment of a stack of

184  Site 1267 and 1264 benthic $\delta^{18}O$ data for the past ~3.6 Ma to the LR04 (Bell et al.,

185  2014). To improve this age model for MIS M2 and the last glacial-Holocene, we

186  supplemented the previously published benthic $\delta^{18}O$ stratigraphy for Site 1267 by

187  generating new $\delta^{18}O$ data between 0-0.34 mcd (n = 16) and 40.27-41.22 mcd (n = 50)

188  and tuned the new resultant stratigraphies to the LR04 (Supplementary Information

189  Section S2).

190

191  2.2. Stable isotope preparation and analysis

192  To generate new benthic foraminiferal stable isotope data ($\delta^{18}O$ and $\delta^{13}C$) for our

193  target intervals, individual tests of the epifaunal species *Cibicidoides wuellerstorfi*

194  (typically n>8) were picked from the 150-400 μm size fraction in 66 samples from

195  Site 1267 (the same samples used to generate Nd isotope data for MIS M2, MIS 100

196  and the last glacial-Holocene) and from the 212-500 μm fraction in 73 samples from

197  the secondary splice of Site U1313 (typically >8 tests per sample, the same samples

198  used to generate Nd isotope data for MIS 100). After drying, picked individuals were

199  cracked open and ultrasonically cleaned in methanol. This was done to remove

200  adhering clays and any low $\delta^{18}O$ clay infilling before a homogenised aliquot was

201    transferred to reaction vials and analysed using a Thermo Finnigan MAT 253 dual

202    inlet mass spectrometer equipped with a Kiel IV Carbonate Device at NOCS,

203    University of Southampton. Data were calibrated using a two-point calibration to

204    standards NBS 18 and 19. We also measured an internal standard (GS1) in each run as

205    a quality control measure that yielded an analytical precision of 0.08‰ for $\delta^{18}O$ and

206    0.02‰ for $\delta^{13}C$ (at 2 s.d.) during the study period. Results are reported relative to the

207    Vienna Peedee belemnite (VPDB) standard. Where the samples picked for stable

208    isotope analysis were also used to generate benthic B/Ca data (e.g., from Site 1267, n

209    = 56), the tests of the picked foraminifera were gently broken open and mixed before

210    being split into two aliquots.

211

212    2.3. Nd-isotope preparation and analysis

213    The local Nd-isotope composition of bottom-water is reliably preserved in fossilised

214    fish tooth, bone and scale hydroxyfluorapatite (henceforth fish debris) during early

215    stage diagenesis, and is resistant to alteration on multi-million year timescales (Martin

216    and Scher, 2004). To develop new Nd isotope datasets, we hand-picked ~50-200 mg

217    of fish debris (10 to 30 pieces of bones and teeth) from the >150 μm fraction of Site

218    U1313 samples and from the >38 μm fraction of Site 1267 samples. Fish debris was

219    cleaned with two steps of ultrasonication in methanol, followed by three steps in

220    Milli-Q 18.2 MΩ·cm water. Organic material was removed by bathing each sample in

221    a buffered oxidising solution (1% $H_2O_2$ – 0.1M $NH_4OH$) at 80$^{\circ}$C for 30 minutes, and

222    sonicated for 30 seconds every 10 minutes. Finally, a weak-acid (0.001M $HNO_3$)

223    polish was applied to ensure removal of any reabsorbed contaminants before samples

224    were dissolved in 0.1ml 1.75M HCl.

225       Pure samples of Nd were extracted from our dissolved samples using a two-

226    stage column procedure. First the rare earth element (REE) fraction was separated

227    using Eichrom TRUspec resin, then Nd was separated from the REE fraction using

228    Eichrom LNspec resin. The $^{143}$Nd/$^{144}$Nd ratio was determined at the University of

229    Southampton using a multi-collector inductively coupled plasma mass spectrometer

230    (MC-ICP-MS, Thermo Scientific Neptune). Neodymium isotopic compositions were

231    obtained using the method of Vance and Thirlwall (2002) through adjustment to a

232    $^{146}$Nd/$^{144}$Nd ratio of 0.7219 and a secondary normalization to $^{142}$Nd/$^{144}$Nd = 1.141876.

233    Mass-bias corrected ratios were normalised to the given $^{143}$Nd/$^{144}$Nd of the standard

234    JNdi-1 (0.512115 (Tanaka et al., 2000)). Total procedural blanks averaged 35 pg

235    during the analysis of our U1313 fish debris. Long-term replication of the JNdi-1

236    standard during this time yielded $^{143}$Nd/$^{144}$Nd = 0.512118 ± 0.000006 (2 s.d.), giving

237    an external reproducibility of 0.13 $\varepsilon_{Nd}$ (2 s.d). Total procedural blanks averaged 39 pg

238    during the analysis of our 1267 fish debris. Long-term replication of the JNdi-1

239    standard during this time yielded $^{143}$Nd/$^{144}$Nd = 0.512116 ± 0.00001 (2 s.d.), giving an

240    external reproducibility of 0.18 $\varepsilon_{Nd}$ (2 s.d). In all cases we report the external

241    uncertainty, unless the internal error is larger than the external error when we plot a

242    combined error calculated as $\sqrt{(\text{external error}^2 + \text{internal error}^2)}$. All Nd isotope

243    ratios are reported in epsilon notation (DePaolo and Wasserburg, 1976) as:

$$\varepsilon_{Nd} = \left[ \frac{^{143}Nd/^{144}Nd_{sample}}{^{143}Nd/^{144}Nd_{CHUR}} - 1 \right] \times 10^4$$

244

245

246

247    Radiogenic in-growth of $^{143}$Nd is corrected following (DePaolo and Wasserburg,

248    1976) using a crustal $^{147}$Sm/$^{144}$Nd value of 0.125 (MacLeod et al., 2008). Such age-

249    corrections are minor (<0.05 $\varepsilon_{Nd}$ for our late Pliocene-earliest Pleistocene data, and

250    <0.0004 $\varepsilon_{Nd}$ for last glacial-Holocene data), reflecting the young age of our samples

251    relative to the half-life of [147]Sm. We note that fish debris and authigenic Fe-Mn

252    oxyhydroxide [147]Sm/[144]Nd typically varies within a narrow range (e.g., 0.121-0.136

253    (Martin et al., 2010)) and that our results are insensitive to the choice of value. The

254    sensitivity of our stated values to application of the range of [147]Sm/[144]Nd = 0.121-

255    0.136 (Martin et al., 2010) is always <0.01 $\varepsilon_{Nd}$, which is negligible.

256

257    2.4 Fresh volcanic glass counts

258    The $\varepsilon_{Nd}$ signal recorded by fish debris can be modified by partial dissolution of fresh

259    radiogenic basaltic volcanic glass by sediment pore waters post deposition (Du et al.,

260    2016). It has been suggested that young volcanic glass sourced from the nearby

261    Azores volcanic island eruptions may have influenced the $\varepsilon_{Nd}$ signal recorded at

262    U1313 during the Holocene (Blaser et al., 2016). To evaluate whether porewater

263    volcanic glass dissolution may have played a role in the trends documented in our Site

264    U1313 $\varepsilon_{Nd}$ data we determined the concentration of fresh volcanic glass (>63 $\mu m\ g^{-1}$)

265    in 53 of the Site U1313 samples analysed in this study and by Lang et al. (2016) for

266    fish debris $\varepsilon_{Nd}$ using a standard method (e.g., Bond and Lotti, 1995).

267      It has been suggested that increased inputs of detrital carbonate sourced from

268    the Canadian Shield (Hudson Bay) to Site U1313 during Heinrich events are

269    responsible for millennial-scale unradiogenic excursions in authigenic $\varepsilon_{Nd}$ at this site

270    (e.g., Lang et al., 2016; Du et al., 2020). Yet, Heinrich layer deposition at Site U1313

271    was restricted to the past ~640 kyr (Naafs et al., 2014). Furthermore, IRD

272    accumulation rates at U1313 are extremely low during ambient glacial conditions

273    over the past ~3.3 Myr (Lang et al., 2014; Lang et al., 2016).

274

275      2.5 Benthic foraminiferal boron/calcium ratios

276      Between 8 and 12 *C. wuellerstorfi* tests (212-500 µm) were cleaned for trace metal

277      analysis from 56 samples from Site 1267 spanning MIS M2, MIS 100 and the last

278      glacial-Holocene following Chalk et al. (2019). Foraminiferal tests were cracked open

279      and ultrasonicated several times in Milli-Q 18.2 MΩ·cm water to remove clay

280      materials. Samples were then oxidatively cleaned in a $NH_3OH$ buffered 1% hydrogen

281      peroxide solution before a 0.0005M weak acid leach was applied to remove adsorbed

282      cations. Finally, samples were dissolved in ~0.075 M nitric acid. The above steps

283      were all undertaken in the boron-free clean laboratory at the University of

284      Southampton. Element ratios were measured using a ThermoFisher Scientific Element

285      2XR-ICPMS at Southampton, using the protocol described by Rae et al. (2011)

286      employing matrix-matched in-house standards and a variety of consistency standards

287      to ensure reproducibility. Samples were screened for clay contamination using Al/Ca

288      and other contaminant ratios (e.g., Ba/Ca, Fe/Ca), with samples Al/Ca > 200

289      µmol/mol excluded from this study (n = 4 out of 56). Long-term reproducibility for

290      B/Ca during this study was evaluated using consistency standards analysed during

291      each analytical session and within 4% at 2 s.d. (~2 mmol/mol). Carbonate ion

292      concentrations were calculated using a sensitivity of $\Delta[CO_2^{3-}]$ on B/Ca of 1.14 ±

293      0.048 for *C. wuellerstorfi* (Yu and Elderfield, 2007), and a $[CO_2^{3-}]_{sat}$ calculated from

294      modern local pressure, temperature and salinity (see Supplementary Information

295      Section S3). The influence of this assumption on the calculated $\Delta[CO_2^{3-}]$ is very

296      small (<0.5 umol/kg; Yu and Elderfield, 2007).

297

298      2.6 Water-mass geochemical end-members

299      We focus on relative change in water-mass composition between different glacials

300  rather than absolute changes but, nevertheless, consider the potential for change in

301  end-member compositions of NCW and SCW. To monitor the $\delta^{13}C$ of NCW during

302  our three target intervals, we use benthic $\delta^{13}C$ data from shallow northeast ODP Site

303  982 (1145 m water depth; Venz et al., 1999). The question of how best to monitor the

304  $\delta^{13}C$ of SCW is more contentious. Sequences recovered from areas ideally located to

305  monitor the end-member composition of SCW (e.g., in the Atlantic sector of the

306  Southern Ocean) are carbonate-poor. Because of this issue, one pioneering study used

307  benthic $\delta^{13}C$ from mid-latitude South Atlantic ODP Site 1090 (~3700 m water depth)

308  for this purpose for the Plio-Pleistocene (Venz and Hodell, 2002). We now know,

309  however that, today and in the past, Site 1090 is partially bathed by NCW (Pena and

310  Goldstein, 2014) making it ill-suited for this purpose. We therefore follow Raymo et

311  al. (1990) and Oppo et al. (1995) and use the $\delta^{13}C$ of Pacific deep water (equatorial

312  Pacific ODP Site 849 (3851 m water depth; Mix et al., 1995) as a conservative, albeit

313  aged, record of the end-member composition of SCW. However, we also compare

314  benthic $\delta^{13}C$ data from our study sites to the benthic $\delta^{13}C$ stratigraphy of Southwest

315  Pacific ODP Site 1123 (3290 m water depth, Fig. S1; Patterson et al., 2018), which is

316  bathed today by a mixture of Antarctic Bottom water and Lower Circumpolar Deep

317  Water. While its Plio-Pleistocene benthic $\delta^{13}C$ stratigraphy shows that the

318  composition of SCW bathing the deep Atlantic has changed over the period of our

319  study interval, it also confirms that marked differences persisted in the $\delta^{13}C$ of NCW

320  and SCW during cold stages over the past 3.6 Ma. The $\delta^{13}C$ of Site 1123 is thought to

321  have decreased from 3.6 Ma in response to increased carbon remineralisation in SCW

322  caused by Southern Ocean sea-ice expansion and a reduction in deep ocean

323  ventilation (Patterson et al., 2018).

324      Knowledge of the $\epsilon_{Nd}$ of NCW and SCW endmembers during the Plio-

Pleistocene, as well as the validity of using fish debris Nd isotope records to

reconstruct water-mass mixing in the deep Atlantic over this time, is comprehensively

discussed in Lang et al. (2016). Briefly, despite their extremely slow precipitation

rates, our best source of information on the evolution of the Nd isotope composition

of NCW and SCW during the Plio-Pleistocene arguably remains the $\varepsilon_{Nd}$ of Fe-Mn

crusts. To estimate the $\varepsilon_{Nd}$ of these water-masses during MIS M2 and MIS 100, we

therefore followed Lang et al. (2016) and took the average value of all published

northwest Atlantic Fe-Mn crust $\varepsilon_{Nd}$ data and their 2 s.d. that span ~3.3-2.4 Ma (from

BM1969.05, ALV539 2-1 and TR079-D14; see supplementary Table S7). For the last

glacial-Holocene, following the approach of Piotrowski et al. (2005), NCW $\varepsilon_{Nd}$ was

defined as the average of previously published Holocene data (<14 ka, MIS 2/1

boundary as defined by Lisiecki and Raymo (2005)) and their 2 s.d. for Site U1313

(Lang et al., 2016). We also define the SCW end-member $\varepsilon_{Nd}$ for all our time target

intervals using the $\varepsilon_{Nd}$ crust record D18-1 from the Indian Ocean Sector of the

Southern Ocean (see supplementary Table S7).

Traditionally, near-consistency in the NCW and SCW end members on orbital

timescales is widely assumed in Nd isotope studies of water-mass mixing (e.g.,

Piotrowski et al., 2005; Böhm et al., 2014; Howe et al., 2016; Lippold et al., 2016).

Yet, recently published records (Wilson et al., 2014; Roberts and Piotrowski, 2015;

Hu et al., 2016; Pöppelmeier et al., 2018; 2019a; Pöppelmeier et al., 2019b; Zhao et

al., 2019; Huang et al., 2020) and numerical modelling studies (e.g., Gu et al., 2019;

Du et al., 2020), raise the possibility that NCW and SCW $\varepsilon_{Nd}$ may have changed, at

least, between the Last Glacial Maximum and the Holocene. In particular, the $\varepsilon_{Nd}$ of

cores from the New England slope at ~1800 m depth (KNR198), a region that should

have been bathed in NCW throughout the Last Glacial Maximum-Holocene, suggest

350    that the preformed composition of NCW may have been up to ~4 ε-units more

351    positive than today during the Last Glacial Maximum (Zhao et al., 2019). In this

352    revised framework, radiogenic excursions in $\varepsilon_{Nd}$ in the deep North Atlantic during the

353    Last Glacial Maximum may reflect changes in the end-member composition of NCW

354    rather than SCW incursion (Zhao et al., 2019; Pöpplemeir et al., 2020; Du et al.,

355    2020). One interpretation of these signals is that higher $\varepsilon_{Nd}$ in the deep North Atlantic

356    during the Last Glacial Maximum (by ~3.5 ε-units, e.g., Böhm et al., 2015; Lang et

357    al., 2016) reflects a reduction in chemical weathering of old unradiogenic cratonic

358    rocks on Canada and Greenland under extensive northern hemisphere ice-sheets and

359    that, when end-member changes are taken into account, the deep North Atlantic

360    remained bathed in near 100% NCW with northward expansion of SCW limited to the

361    deep South Atlantic (Zhao et al, 2019; Pöppelmeier et al., 2020).

362         The plausibility of temporal variations in NCW $\varepsilon_{Nd}$ being driven by chemical

363    weathering has recently been challenged by Du et al. (2020) from a tracer budget

364    perspective. The notion that the extent of chemical weathering on North America

365    controls the $\varepsilon_{Nd}$ of NCW is also challenged by North Atlantic crust records which

366    demonstrate that, as ice-sheet coverage of high northern latitude Archean and

367    Proterozoic cratons increased over the past 3.3 Myr, the long-term Nd isotope

368    composition of NCW has decreased (Burton et al., 1999; Vance and Burton, 1999;

369    Reynolds et al., 2004). A dominant role for chemical weathering is also hard to

370    reconcile with the fact that Site U1313 $\varepsilon_{Nd}$ appears to vary in phase with southern (not

371    northern) hemisphere insolation, especially prior to 2.7 Ma (Supplementary Figure

372    S6). An alternative interpretation of the high $\varepsilon_{Nd}$ values in the North Atlantic during

373    the Last Glacial Maximum is that they reflect a reduction in the contribution to NCW

374    of unradiogenic Labrador Seawater (Hillaire-Marcel et al., 2001a; 2001b) and a shift

15

375  in the location and mode of NCW formation to south of Iceland (Sarnthein et al.,

376  1994) where its preformed composition is made more positive by 'bottom-up' non-

377  conservative processes (i.e., partial dissolution of radiogenic authigenic (volcanic)

378  phases) enhanced by a more sluggish glacial circulation (Du et al., 2020). Given

379  these uncertainties, we proceed with caution herein, assuming near-consistency in Nd

380  end-members on orbital timescales (the traditional interpretive framework), but also

381  discuss the implications of this revised framework.

382

383  **3 Results and Discussion**

384  **3.1. Nd isotopes and B/Ca ratios**

385  In Figures 3 and 4 we integrate new and published data to present high resolution

386  records of fish debris-derived $\varepsilon_{Nd}$ and B/Ca and $\delta^{13}C$ in benthic foraminiferal calcite

387  for the deep Atlantic Ocean during MIS M2, ~3.3 Ma, MIS 100, ~2.52 Ma, and the

388  last glacial-Holocene, ~40-0 ka. Our reconstruction of $\varepsilon_{Nd}$ and $[CO_3^{2-}]$ in bottom-

389  waters bathing Site 1267 during the latest Holocene (averages = ~ −10.7±0.2 and

390  93±10 μmol kg$^{-1}$) are strikingly similar to those reported for LDW bathing Walvis

391  Ridge in the Angola Basin today ($\varepsilon_{Nd}$ = −10.6±0.7; 30˚S 1˚W, 4675 m water depth

392  (Jeandel, 1993) and $[CO_3^{2-}]$ = ~100 μmol kg$^{-1}$ (Lauvset et al., 2016)) strongly

393  suggesting that our data from this site faithfully track changes in deep water-mass

394  mixing in the Angola Basin (also see Supplementary Information Section 5).

395      The magnitude of peak interglacial-full glacial change in $[CO_3^{2-}]$, $\varepsilon_{Nd}$ and

396  benthic $\delta^{13}C$ at Site 1267 is comparable between all three of our studied time

397  windows (with average IG-G change of ~10-22 μmol kg$^{-1}$, ~0.7-1.9 ε-units and ~0.4-

398  0.5 ‰, respectively; data in red in Fig. 3d-l; Tab. 1). The new highly resolved Nd

399  isotope record from Site U1313 for MIS 100 confirms the last glacial-magnitude shift

16

400    in $\varepsilon_{Nd}$ (~1.85 for peak interglacial to full glacial; data in black and grey in Fig. 3h;

401    Tab. 1) inferred from a less well resolved record (data in grey in Fig. 3h; Lang et al.,

402    2016). The new high-resolution record for MIS M2 at Site U1313 also shows that,

403    while there is a prominent short-term maximum in $\varepsilon_{Nd}$ during the early glacial phase

404    of M2 (~3.305 Ma, labelled EG in Fig. 3i), by the time full glacial (FG) conditions are

405    reached at this site, $\varepsilon_{Nd}$ is only ~0.7 $\varepsilon$-units higher on average than during the

406    preceding interglacial MIS MG1 (Tab. 1). No analogous early glacial short-term

407    structure in $\varepsilon_{Nd}$ is documented in the corresponding benthic $\delta^{13}C$ record for MIS M2

408    (compare data in grey in Fig. 3i to 3l). The magnitude of change in benthic $\delta^{13}C$ at

409    Site U1313 is small throughout MIS M2 (average IG-G change of only ~0.2 ‰)

410    relative to both MIS 100 (average IG-G change of ~0.75 ‰) and the last glacial-

411    Holocene (average IG-G change of ~0.55 ‰).

412

413    **3.2. Deep Atlantic Ocean structure during the Last Glacial-Holocene**

414    Our data reveal distinct geochemical differences between bottom waters at Site 1267

415    (today bathed in 70-80% lower NADW) and Site U1313 (today bathed in 100% lower

416    NADW) in $\varepsilon_{Nd}$, benthic $\delta^{13}C$ and $[CO_3^{2-}]$ over the past ~10 kyr (>+2 $\varepsilon$-units, -0.3 ‰

417    and ~−20 µmol kg$^{-1}$, respectively) (Fig. 4a, d, j). These observations demonstrate that

418    SCW influenced bottom-waters bathing the northern flank of Walvis Ridge

419    throughout the Holocene. Our $[CO_3^{2-}]$ estimates for MIS 2 at Site 1267 (data in red in

420    Fig. 4a) are comparable to those reported for the deep northeast North Atlantic (e.g.,

421    IODP Site U1308 at 51˚N and ~3800 m depth, data in dark blue in Fig. 4a) but they

422    are ~80 µmol kg$^{-1}$ lower than those estimated for the mid-depth northeast North

423    Atlantic (e.g., ODP Site 980 at 55˚N and ~2170 m depth, data in green in Fig. 4a).

424    The new $[CO_3^{2-}]$ estimates from Site 1267 therefore also show that the pronounced

425  carbonate-system depth-stratification reconstructed (e.g., by Yu et al., 2008; Chalk et

426  al., 2019) for the eastern Atlantic basin during the last glacial (compare $[CO_3^{2-}]$ 980

427  data in green with U1308 and 1267 data in dark blue and red, respectively, in Fig. 4a)

428  probably extended southwards to Walvis Ridge (at ~30˚S). The new data are also

429  consistent with the suggestion (Chalk et al., 2019) that the dissolved inorganic carbon

430  (DIC) contents of the deep eastern Atlantic, at depths >3800 m, may be larger than

431  those of contemporaneous deep waters in the western Atlantic (compare data in red,

432  dark blue and black in Fig. 4a).

433      The simplest explanation for the radiogenic $\varepsilon_{Nd}$, low benthic $\delta^{13}C$ and low B/Ca

434  ratios in our MIS 2 datasets for Site 1267 is that they reflect an increased influence of

435  SCW on deep-waters bathing Walvis Ridge in the Angola Basin relative to the

436  Holocene. This explanation holds true even when recent assumptions about potential

437  changes in NCW and SCW during the Last Glacial Maximum (e.g., Zhao et al., 2019;

438  Pöppelmeier et al., 2020) are considered because our Site 1267 $\varepsilon_{Nd}$ are still more

439  radiogenic than those recorded at Site KNR198, a recently proposed record of

440  preformed NCW for the Last Glacial Maximum (Zhao et al., 2019); Fig. 4d). In this

441  explanation, the pathway for SCW to the Angola Basin is the Romanche Fracture

442  zone, which today provides an equatorial passageway for SCW to this basin down to

443  4350 m (labelled RFZ in Fig. 2). This fracture zone was recently invoked as a route

444  for SCW during MIS 2 and used to explain low $[CO_3^{2-}]$ in bottom waters bathing the

445  northeast North Atlantic (Site U1308 at 51˚N) during this time (Chalk et al., 2019).

446  As in the modern, the Vema Fracture Zone (VFZ), situated further north but in even

447  deeper water (~5000 m) (Fig. 2; Demidov et al., 2006) provides an even more

448  effective conduit for SCW flow to reach the northeast North Atlantic during Plio-

449  Pleistocene glacials. The deeper VFZ may help explain why bottom waters bathing

450    Site U1308 during the Last Glacial Maximum have lower $[CO_3^{2-}]$ than those bathing

451    Site 1267.

452        Today, the $[CO_3^{2-}]$ of deep-waters can be used as a quasi-conservative tracer of

453    water-mass source, but this may not have been the case during MIS 2. A variety of

454    processes unrelated to water-mass mixing can modify the $[CO_3^{2-}]$ of the ocean (e.g.,

455    air-sea exchange, alkalinity change and biological processes), but given that $[CO_3^{2-}]$

456    will react differently to these processes compared to $\delta^{13}C$, paired $[CO_3^{2-}]$-$\delta^{13}C$ data

457    can be used to determine whether changes in the former reflect changes in water-mass

458    structure or non-conservative processes (e.g., Yu et al. 2008; Chalk et al., 2019). The

459    trend of paired $[CO_3^{2-}]$-$\delta^{13}C$ data from Site U1308 for the last glacial and Holocene

460    approximates best to a trend line indicative of $CO_2$ influx (e.g., of ocean uptake of

461    carbon), indicating carbonate system proxy data can be used at this site as a quasi-

462    conservative tracer of SCW-NCW mixing (small black filled and hollow circles in

463    Fig. 5a). By contrast, the gradients of paired $[CO_3^{2-}]$-$\delta^{13}C$ data from sites 1267 and

464    U1313 for the same time interval in $\delta^{13}C$-$[CO_3^{2-}]$ space is significantly steeper (solid

465    and hollow green and red circles in Fig. 5a) and better approximate the slope of the

466    'biology line' of Yu et al. (2008). This observation indicates that carbon

467    remineralization may have contributed to the paired low $\delta^{13}C$ and $[CO_3^{2-}]$ values at

468    sites 1267 and U1313 during MIS 2 (by decreasing the $\delta^{13}C$ of DIC bathing 1267 and

469    U1313 beyond that anticipated from linear mixing of SCW-NCW alone).

470    Nevertheless, an increase in the contribution of SCW to these two sites relative to the

471    Holocene is indicated by our $\varepsilon_{Nd}$ records (Fig. 4d).

472        Dense Norwegian-Greenland Sea (NGS) overflows are proposed to contribute

473    to the deep waters bathing Walvis Ridge throughout much of the Pleistocene (Bell et

474    al., 2014; 2015). This suggestion invokes a deep Eastern Atlantic route for this water-

475   mass to the Angola Basin. This possibility cannot be ruled out for our study intervals

476   based on our $\varepsilon_{Nd}$ data alone because today both Nordic Sea overflows and AABW

477   share a radiogenic $\varepsilon_{Nd}$ signature (of $\sim -7$ to $-9$; Crocker et al., 2016). Yet $[CO_3^{2-}]$ is

478   markedly higher for modern NGS overflow water ($>115$ µmol kg$^{-1}$) than for SCW

479   ($\sim 85$ µmol kg$^{-1}$) and this contrast would have been greater during the Last Glacial

480   Maximum than today (Yu et al., 2008; Crocker et al., 2016). Thus, it is unlikely that

481   the radiogenic ($\varepsilon_{Nd} = -9$, Fig. 4d-e) and $[CO_3^{2-}]$ low ($= \sim 80 \pm 10$ µmol kg$^{-1}$, Fig. 4a-b)

482   deep-waters bathing Site 1267 during the MIS 2 and MIS 100 were composed of

483   dense overflow waters sourced directly from the NGS via an abyssal eastern basin

484   route. This is a robust interpretation even if their composition was overprinted en

485   route by extensive biological remineralization of carbon.

486

487   **3.3. Deep Atlantic Ocean structure during MIS M2 and 100**

488   The consistency in the amplitude of IG-G change in all three water-mass proxies at

489   Site 1267 during all three of our target time slices (Tab. 1) suggests that the

490   oceanographic response to MIS M2, MIS 100 and MIS 2 in the deep South Atlantic

491   was similar across all three glacials, i.e., all proxies reflect an increase in the influence

492   of SCW. In contrast, IG-G changes in $\delta^{13}C$ and $\varepsilon_{Nd}$ at Site U1313 suggest a smaller

493   contribution of SCW to deep waters bathing this shallower more northerly situated

494   site during MIS M2 than during MIS 100 and MIS 2 (Tab. 1).

495       The validity of this conclusion depends on there not being major changes in the

496   offset between the end-member compositions of NCW and SCW during these times.

497   A last-glacial-Holocene-like change in $\varepsilon_{Nd}$ at Site 1267 during MIS M2 and MIS 100

498   could be artificially produced by a more positive SCW $\varepsilon_{Nd}$ during these cold stages

499   relative to MIS 2. Because SCW is a mixture of relatively unradiogenic Atlantic and

500     radiogenic Pacific waters (Stichel et al., 2012) a more positive SCW could arise in

501     two ways. First, if the composition and mixing contribution of the Pacific end-

502     member to SCW remained similar during our three studied glacials, a more positive

503     NCW would lead to a more positive SCW when it mixes with Pacific deep waters in

504     the Southern Ocean. Second, SCW could become more positive if NCW makes a

505     smaller contribution to SCW due to a reduction in the southward advection rate of

506     North Atlantic deep waters. Based on the available crust data (Frank et al., 2002), it is

507     reasonable to assume that the $\varepsilon_{Nd}$ composition of the Pacific end-member remained

508     stable during our study intervals, but the Nd isotope composition of NCW did not

509     (compare red and blue horizontal bars in Fig. 4d-f). Both the crust records and Site

510     U1313 $\varepsilon_{Nd}$ illustrate that NCW was ~1 $\varepsilon$-unit more radiogenic during the late Pliocene

511     than it was during the late Pleistocene (Fig. 4d-f). Yet, a relatively radiogenic NCW

512     during MIS 100 and MIS M2 would not have changed the gradient in $\varepsilon_{Nd}$ between

513     NCW-SCW during these cold stages relative to MIS 2 because it would also have

514     made SCW more radiogenic. We can also rule out the possibility that a reduction in

515     the southward advection rate of NCW relative to MIS 2 could explain the existence of

516     a last-glacial-Holocene-like change in $\varepsilon_{Nd}$ at Site 1267 during MIS M2 and MIS 100

517     because it is unlikely that Atlantic Meridional Overturning Circulation (AMOC)

518     weakening was greater during late Pliocene and earliest Pleistocene cold stages than

519     during MIS 2.

520        Our interpretations of relative changes in our water-mass proxy data are

521     supported by a comparison between the benthic $\delta^{13}C$ data from our study sites and the

522     well-constrained $\delta^{13}C$-based estimates of NCW and SCW end members (Fig. 4j-l). A

523     comparison of benthic $\delta^{13}C$ values at Site 1267 to those at Site 982 (the NCW end-

524     member) reveals that there was an increased contribution of SCW bathing Walvis

525    Ridge for most of early- to mid-glacial M2 until ~3295 ka (compare data in red and

526    purple in Fig. 4l). While our knowledge of NCW and SCW $\varepsilon_{Nd}$ during MIS M2 is less

527    certain, our Nd isotope data from this site record the same history of SCW incursion

528    during this cold stage as inferred from benthic $\delta^{13}C$ (compare data in red and orange

529    in Fig. 6d). In contrast, at Site U1313, benthic $\delta^{13}C$ values are comparable to those of

530    NCW throughout MIS M2 (compare data in black and purple in Fig. 4l). We infer

531    that, while SCW contributed significantly to the deep waters bathing Site 1267 during

532    this glacial at least until ~3295 ka, Site U1313 was mainly bathed by NCW during

533    MIS M2. We note the radiogenic spike in Nd during early MIS M2 (star in Fig. 4f)

534    but find no supporting evidence that it arises from water-mass mixing (see

535    supplementary information Section S6).

536

537    3.3.1 What would be the implication of changing $\varepsilon_{Nd}$ end members for

538    our interpretation of MIS M2?

539    We have interpreted the history of deep Atlantic Ocean structure using the traditional

540    framework wherein the end-member $\varepsilon_{Nd}$ compositions of NCW and SCW did not

541    change appreciably on glacial-interglacial timescales (e.g., Foster et al., 2007;

542    Piotrowski et al., 2005; Böhm et al., 2015; Howe et al., 2016). If major end-member

543    change in NCW occurred over the last glacial cycle (of ~+4 ε-units) then it is possible

544    that the deep North Atlantic remained bathed in near 100% NCW during the Last

545    Glacial Maximum and northward expansion of SCW was limited to the deep South

546    Atlantic (Zhao et al, 2019; Pöppelmeier et al., 2020). However, an absence of SCW in

547    the deep North Atlantic during the Last Glacial Cycle is hard to reconcile with the fact

548    that benthic $\delta^{18}O$ from, e.g., the Iberian Margin correlates so well with Antarctic

549    temperature (Shackleton et al., 2000). Nevertheless, in this scenario, the large

550    negative excursion recorded in North Atlantic benthic $\delta^{13}C$ records during the Last

551    Glacial Maximum is proposed to reflect enhanced remineralisation of carbon in deep-

552    waters (Howe et al., 2016) under a more sluggish (i.e., diminished AMOC) glacial

553    deep Atlantic circulation relative to modern (Böhm et al., 2015; Ng et al., 2018).

554        What would be the implication for our interpretation of MIS 100 and M2 if this

555    alternative framework is correct? There are two suggested mechanisms for NCW end-

556    member change. In the first case, change is driven by chemical weathering extent on

557    North America (Zhao et al., 2019; Pöppelmeier et al., 2020) such that deep North

558    Atlantic $\varepsilon_{Nd}$ acts as a proxy of Plio-Pleistocene North American Ice Sheet extent. In

559    this case, the large radiogenic $\varepsilon_{Nd}$ excursions during MIS 2 and MIS 100 at Site

560    U1313 (Lang et al., 2016; this study; Fig. 3g-h; Tab. 1) signal comparable reductions

561    in chemical weathering on North America and Greenland due to a similar spatial

562    configuration of ice-sheets on Canada and Greenland whereas the relatively

563    unradiogenic $\varepsilon_{Nd}$ values during MIS M2 point to more limited glaciation of North

564    American and Greenland (Lang et al., 2016; this study; Fig. 3g-i; Tab. 1). The second

565    mechanism for large radiogenic $\varepsilon_{Nd}$ excursions involves relabelling of NCW via

566    partial dissolution of east Greenlandic- and Icelandic-sourced radiogenic volcanic

567    phases deposited in the Iceland basin, following a shift in the location of the main site

568    of NCW formation from the sea ice-covered Nordic Seas to south of Iceland, and a

569    reduction in unradiogenic Labrador Seawater production (Du et al., 2020). In this

570    case, our data for MIS 2 and MIS 100 signal a slowdown in AMOC (reduced bottom

571    current speeds in the Iceland Basin promotes labelling via partial dissolution of

572    volcanic phases because the longer benthic exposure time that results allows seawater

573    and authigenic $\varepsilon_{Nd}$ in this region to converge toward detrital sediment $\varepsilon_{Nd}$ (Du et al.,

574    2020)), whereas the muted IG-G shift in $\varepsilon_{Nd}$ at Site U1313 during MIS M2 (Tab. 1)

575 signals vigorous formation of NCW in largely ice-free Nordic and Labrador seas.

576 Either way, if radiogenic excursions in the deep North Atlantic during glacials reflect

577 end-member changes in NCW $\varepsilon_{Nd}$, the lack of a large negative excursion in Site

578 U1313 benthic $\delta^{13}C$ during MIS M2 (compare data in red in Fig. 3l and 3g-h; Tab. 1)

579 implies reduced remineralisation of $^{12}C$ in the deep North Atlantic relative to the Last

580 Glacial Maximum and MIS 100 under a more vigorous AMOC (Pöppelmeier et al.,

581 2020). Thus, regardless as to whether our North Atlantic $\varepsilon_{Nd}$ records reflect changes in

582 water-mass provenance or a change in the preformed composition of NCW, they

583 strongly suggest that Atlantic Ocean circulation during MIS M2 was markedly

584 different to that of large Quaternary glaciations with markedly weaker chemical

585 stratification.

586

587 **3.4 Implications for glacial $CO_2$-storage in the ocean abyss**

588 A ~110 ppm decline in atmospheric $CO_2$ during MIS M2 (Fig. 6a) strongly implies

589 increased carbon storage in the abyssal ocean (de la Vega et al., 2020). A Southern

590 Ocean-focused driving mechanism is favoured by de la Vega et al. (2020) because the

591 tail end of the $CO_2$ decline documented appears out of phase with the decline in

592 northern hemisphere insolation and benthic $\delta^{18}O$ but in-phase with both insolation

593 decline at 65°S (compare $CO_2$ record in Fig. 6a to data in black in 6b,f) and Nd

594 isotope-based evidence for SCW incursion into the North Atlantic (Lang et al. (2016)

595 (compare Fig. 6a to U1313 $\varepsilon_{Nd}$ data points denoted by grey boxes in 6c). Yet, in

596 contrast to previous suggestions (e.g., Lang et al., 2016), we find that SCW expansion

597 during MIS M2 was limited to the deep South Atlantic (as tracked by 1267). Our data

598 also suggest that this modest SCW expansion in the Atlantic during MIS M2 peaked

599 ~10-15-kyr before minimum values in atmospheric $CO_2$ were reached during this

600　glacial (compare red horizontal bar in Fig. 6d to $CO_2$ data in 6a). Together, these

601　observations imply that the deep Atlantic was not the ultimate store for the $CO_2$

602　sequestered from the atmosphere during this cold stage. Future work should focus on

603　the possibility that the deep Pacific played a major $CO_2$ storage role, as hinted at by

604　the temporal relationship between benthic $\delta^{13}C$ at Site 1123 and atmospheric $CO_2$

605　during MIS M2 (compare Fig. 6a to 1123 $\delta^{13}C$ data in blue in 6d).

606

607　**3.5 How sluggish was AMOC during MIS M2?**

608　The lag between atmospheric $CO_2$ and benthic $\delta^{18}O$ during MIS M2 (Section 3.4)

609　implies that high latitude cooling and glaciation during this cold stage were not

610　simply controlled by radiative forcing from greenhouse gases. Instead, other

611　mechanisms must have been important. One mechanism invoked to have played at

612　least a part in amplifying glaciation of the high northern latitudes is AMOC

613　weakening (De Schepper et al., 2013).

614　　　　AMOC suppression of a magnitude comparable to that reconstructed for major

615　Quaternary glaciations including the Last Glacial Maximum (e.g., Naafs et al., 2010;

616　Bolton et al., 2018), is invoked for M2 based on evidence from dinoflagellate

617　assemblages for a southward deflection of the North Atlantic Current (NAC) to ~41˚N

618　(see panel '3' in Figure 6 of De Schepper et al., 2013) and significant reductions in

619　North Atlantic SSTs (of up to 6˚C; Fig. 7f). The sediment abundance of the

620　dinoflagellate *Operculodinium centrocarpum*, which has a strong affinity with NAC

621　waters in the modern (De Schepper et al., 2013), in Site U1308 (50˚N) and 610 (53˚N)

622　(Fig. 7g) provide evidence for NAC weakening and/or its deflection south of ~50˚N

623　throughout MIS M2 (Fig 8c). The abundance of *O. centrocarpum* in Site U1313

624　sediments deposited at 41˚N during this cold stage is only high, however, during early

625 glacial conditions (Fig. 7h), indicating that maximum southward deflection of the

626 NAC during this time occurred well before the full glacial MIS M2 (Fig. 8d). An

627 early glacial timing for maximum NAC decline during MIS M2 is consistent with our

628 observation that SCW incursion into the deep Atlantic reached its MIS M2 peak

629 before ~3295 ka (compare Fig. 7b-c to 7h).

630 Palaeoceanographic records suggest that AMOC can remain relatively strong in

631 the face of a significant reduction in the volumetric extent of NCW (e.g., Böhm et al.,

632 2015). Yet, numerical models of ocean circulation indicate that if AMOC vigour

633 during MIS M2 was comparable to the Last Glacial Maximum, it should be associated

634 with a similarly large (i.e., late Pleistocene glacial-like) reduction in the volumetric

635 importance of the NCW overturning cell (e.g., Nikurashin and Vallis, 2011; Kostov et

636 al., 2014; Burke et al., 2015). If changes in $\varepsilon_{Nd}$ at U1313 reflect the magnitude of

637 SCW incursion into the deep North Atlantic during our three target glacials, our new

638 datasets show that M2 was not associated with NCW shoaling on the scale of the last

639 glacial or even MIS 100, 2.52 Ma (Fig. 4d-f, j-l). If the evolution of $\varepsilon_{Nd}$ at U1313

640 instead reflects changes in the preformed composition of NCW (e.g., Zhao et al.,

641 2019; Pöppelmeier et al., 2020), the small amplitude of IG-G change in $\varepsilon_{Nd}$ and

642 benthic $\delta^{13}C$ at this site during MIS M2 would also be inconsistent with a

643 significantly weaker-than-modern AMOC (see Section 3.3.1). Either way, our new

644 records strongly suggest that AMOC during this cold stage was not as sluggish as

645 during major Quaternary glacials.

646 Our interpretations are consistent with the surface temperature history of the

647 North Atlantic. A ~6°C decline in SSTs in the subpolar North Atlantic during MIS

648 M2 provides clear evidence for a reduction in northward heat transport from a

649 warmer-than-pre-industrial baseline but temperatures remained as warm (Sites 982

650   and U1313) or warmer (Sites 642 and 610) than the Holocene average (Fig. 7f). These

651   observations may help us to understand why firm evidence for glacial expansion in

652   the high northern latitudes ~3.3 Ma is limited to circum-Arctic landmasses,

653   Greenland, Svalbard and Iceland (De Schepper et al., 2014; Tan et al., 2017). We note

654   that sediments interpreted as glacial tills from mid-latitude James Bay Lowland,

655   Canada, have been loosely dated to ~3.5 Ma (Gao et al., 2012), but this interpretation

656   has been called into question (Clague et al., 2020).

657

658   **4. Conclusions**

659   We present new Nd isotope data and benthic foraminiferal B/Ca ratios for southeast

660   Atlantic Site 1267 (29˚S, ~4350 m water depth) and northwest Atlantic Site U1313

661   (41˚N, ~3400 m water depth) spanning the last glacial-Holocene, MIS 100, 2.52 Ma,

662   and MIS M2, ~3.3 Ma, often inferred to signal a prelude to Quaternary extensive

663   glaciation of the northern hemisphere and therefore a bi-polar Cenozoic icehouse

664   climate state. We demonstrate that Southern Component Water expanded into the

665   deep South and North Atlantic during MIS 100. The resulting glacial water-mass

666   properties at our study sites are comparable to those that we document for the last

667   glacial. This Quaternary glacial picture contrasts with the one that we document for

668   MIS M2, in which Northern Component Water persists in the deep North Atlantic.

669        Our new observations are incompatible with AMOC suppression during MIS

670   M2 to the scale of MIS 100 or 2 and suggest that the atmospheric $CO_2$ decline during

671   this cold stage was not achieved by carbon storage in the deep Atlantic Ocean,

672   implying storage in deep Pacific Ocean reservoirs. Our findings, together with

673   Holocene-like surface ocean temperatures in the high latitude North Atlantic, help to

674   resolve the mystery of why there is no evidence to suggest that the

675  northern hemisphere was extensively glaciated during M2.

676

690

691  **Data Availability:** The data presented in this manuscript will be made available upon

692  request. These data will be deposited in PANGAEA upon acceptance on this

693  manuscript for publication.

694

695  **Declaration of interests:** none.

696

697  **Author Contributions:** N.K generated the Site 1267 data and contributed to

698  manuscript writing; I.B. designed the study, supervised N.K. in data generation and

699  wrote the manuscript; A.B generated the Site U1313 stable isotope data for MIS 100

28

700 and contributed to manuscript writing; T.B.C. supervised R.L.P in generating the Site

701 1267 benthic B/Ca data and contributed to the ideas presented and to manuscript

702 writing; R.L.P generated a subset of the Site 1267 data; A.J.C. supervised N.K. and

703 R.L.P in data generation, contributed to the ideas presented and to manuscript writing;

704 V.E.T. supervised N.K. and R.L.P. in data generation, generated the volcanic glass

705 count data and contributed to manuscript writing; J.A.M helped to generate the Nd

706 isotope data; G.L.F. contributed to the ideas presented and manuscript writing;

707 M.E.R. contributed to the ideas presented and manuscript writing; D.K. contributed

708 samples and to the ideas presented and manuscript writing; D.B.B contributed

709 samples and to manuscript writing; P.A.W. designed the study, supervised N.K. in

710 data generation, co-wrote the manuscript with I.B.

711

712

713 **6. References**

714 Arhan, M., Mercier, H., Park, Y.-H., 2003. On the deep water circulation of the

715       eastern South Atlantic Ocean. Deep-Sea Research I 50, 889-916.

716       doi:10.1016/S0967-0637(03)00072-4

717 Bachem, P.E., Risebrobakken, B., De Schepper, S., McClymont, E.L., 2017. Highly

718       variable Pliocene sea surface conditions in the Norwegian Sea. Climate of the

719       Past 13 1153-1168, doi:10.5194/cp- 13-1153-2017

720 Bayon, G., German, C.R., Boella, R.M., Milton, J.A., Taylor, R.N., Nesbitt, R.W.,

721       2002. An improved method for extracting marine sediment fractions and its

722       application to Sr and Nd isotopic analysis. Chemical Geology187, 179–199.

723 Bayon, G., German, C.R., Nesbitt, R.W., Bertrand, P., Schneider, R.R., 2003.

724       Increased input of circumpolar deep water-borne detritus to the glacial SE

725           Atlantic Ocean, Geochem. Geophys. Geosyst. 4(3), 1025,

726           doi:10.1029/2002GC000371.

727  Bayon, G., Burton, J.W., Soulet, G., Vigier, N., Dennielou, B., Etoubleau, J.,

728           Ponzevera, E., German, C.R., Nesbitt, R.W.,2009. Hf and Nd isotopes in

729           marine sediments: Constraints on global silicate weathering. EPSL 277, 318–

730           326. doi:10.1016/j.epsl.2008.10.028.

731  Bell, D.B., Jung, S.J.A., Kroon, D., Lourens, L.J., Hodell, D.A., 2014. Local and

732           regional trends in Plio-Pleistocene $d^{18}O$ records from benthic foraminifera.

733           Geochem. Geophys. Geosystems. http://dx.doi.org/10.1002/2014GC005297.

734  Bell, D.B., Jung, S.J.A., Kroon, D., 2015. The Plio-Pleistocene development of

735           Atlantic deep-water circulation and its influence on climate trends. Quaternary

736           Science Reviews 123, 265-282.

737           http://dx.doi.org/10.1016/j.quascirev.2015.06.026.

738  Blaser, P., Lippold, J., Gutjahr, M., Frank, N., Link, J.M., Frank, M., 2016. Extracting

739           foraminiferal seawater Nd isotope signatures from bulk deep sea sediment by

740           chemical leaching. Chemical Geology 439, 189-204.

741           http://dx.doi.org/10.1016/j.chemgeo.2016.06.024.

742  Böhm, E. et al., 2015. Strong and deep Atlantic meridional overturning circulation

743           during the Last Glacial Cycle. *Nature* 517, 73–76.

744  Bolton, C.T., Wilson, P.A., Bailey, I., Friedrich, O., Beer, C.J., Becker, J., Baranwal,

745           S., Schiebel, R., 2010. Millennial- scale climate variability in the subpolar

746           North Atlantic Ocean during the late Pliocene, Paleoceanography 25, PA4218,

747           doi:10.1029/2010PA001951.

748  Bolton, C.T., Bailey, I., Friedrich, O., Tachikawa, K., de Garidel-Thoron, T., Vidal,

749           L., et al., 2018. North Atlantic midlatitude surface-circulation changes

750        through the Plio-Pleistocene intensification of Northern Hemisphere

751        glaciation. Paleoceanography and Paleoclimatology, 33. https://doi.org/

752        10.1029/2018PA003412.

753    Bond, G.C., Lotti, R., 1995. Iceberg discharges into the North Atlantic on millennial

754        time scales during the last glaciation. Science 267, 1005-1010.

755    Brigham-Grette, J. et al., 2013. Pliocene warmth, polar amplification, and stepped

756        Pleistocene cooling recorded in NE Arctic Russia. Science 340,

757        1421–1426.

758    Burke, A., Stewart, A.L., Adkins, J.F., Ferrari, R., Jansen, M.F., Thompson, A.F.,

759        2015. The glacial mid-depth radiocarbon bulge and its implications for the

760        overturning circulation, Paleoceanography 30, 1021–1039,

761        doi:10.1002/2015PA002778.

762    Burton, K.W., Ling, H.F., O'Nions, R.K., 1997. Closure of the Central American

763        Isthmus and its effect on deep-water formation in the North Atlantic. Nature

764        386, 382–385. doi:10.1038/386382a0.

765    Burton, K.W., Lee, D.-C., Christensen, J.N., Halliday, A.N., Hein, J.R., 1999. Actual

766        timing of neodymium isotope variations recorded by FeMn crusts in the western

767        North Atlantic. EPSL 171, 149–156. doi:10.1016/S0012-812X(99)00138-7.

768    Cande, S.C., Kent, D.V., 1995. Revised calibration of the geomagnetic polarity

769        timescale for the Late Cretaceous and Cenozoic. J. Geophys. Res. 1000 (B4),

770        6093–6095.

771    Chalk, T.B., Foster, G.L., Wilson, P.A., 2019. Dynamic storage of glacial $CO_2$ in

772        the Atlantic Ocean revealed by boron $[CO_3^{2-}]$ and pH records. EPSL 510, 1–11.

773    Choboter, P.F., Swaters, G.E., 2000. Modelling equator-crossing currents on the

774        ocean bottom. Canadian Applied Mathematics Quarterly 8(4), 367–385.

775    Clague, J.J., Barendregt, R.W., Menounos, B., Roberts, N.J., Rabassa, J., Martinez,

776        O., Ercolano, B., Corbella, H., Hemming, S.R., 2020. Pliocene and Early

777        Pleistocene glaciation and landscape evolution on the Patagonian Steppe,

778        Santa Cruz province, Argentina. Quat. Sci. Revs. 227, 105992.

779        https://doi.org/10.1016/j.quascirev.2019.105992.

780    Coles, V.J., McCartney, M.S., Olson, D.B., Smethie Jr., W.M., 1996. Changes in

781        Antarctic Bottom Water properties in the western South Atlantic in the late

782        1980s. Journal of Geophysical Research 101, C3. 8957–8970.

783    Connary, S.D., Ewing, M., 1974. Penetration of Antarctic Bottom Water from the

784        Cape Basin into the Angola Basin. Journal of Geophysical Research 79, 463–

785        469.

786    Crocker, A.J., Chalk, T.B., Bailey, I., Spencer, M.R., Gutjahr, M., Foster, G.L.,

787        Wilson, P.A., 2016. Geochemical response of the mid-depth Northeast

788        Atlantic Ocean to freshwater input during Heinrich events 1 to 4. Quaternary

789        Science Reviews 151, 236-254.

790    DeConto, R.M., Pollard, D., Wilson, P.A., Palike, H., Lear, C.H., Pagani, M., 2008.

791        Thresholds for Cenozoic bipolar glaciation. Nature 455, 652–656. http://

792        dx.doi.org/10.1038/nature07337.

793    Demidov, A.N., Morozov, E.G., Neiman, V.G., 2006. Structure and variability of

794        deep waters in the Romanche Fracture Zone Dokl. Earth Sc. 410: 1136.

795        https://doi.org/10.1134/S1028334X06070300.

796    DePaolo, D., Wasserburg, G., 1976. Nd isotopic variations and petrogenetic models.

797        Geophysical Research Letters 3, 249–252. 10.1029/GL003i005p00249.

798    de la Vega, E., Chalk, T.B., Wilson, P.A., Bysani, R.P., Foster, G.L.,2020.

799        Atmospheric $CO_2$ during the Mid-Piacenzian Warm Period and the M2

800       glaciation. Scientific Reports 10, 11002. https:// doi.org/10.1038/s41598-020-

801       67154-8.

802   De Schepper, S., Head, M.J., Groeneveld, J., 2009. North Atlantic Current

803       variability through marine isotope stage M2 (circa 3.3 Ma) during the mid-

804       Pliocene, Paleoceanography 24, PA4206. doi:10.1029/2008PA001725.

805   De Schepper, S., Groeneveld, J., Naafs, B.D.A., Van Renterghem, C., Hennissen, J.,

806       et al., 2013. Northern Hemisphere Glaciation during the Globally Warm Early

807       Late Pliocene. PLoS ONE 8(12): 81508. doi:10.1371/journal.pone.0081508

808   De Schepper, S., Gibbard, P.L., Salzmann, U., Ehlers, J., 2014. A global synthesis of

809       the marine and terrestrial evidence for glaciation during the Pliocene Epoch.

810       Earth-Science Reviews 135. doi:10.1016/j.earscirev.2014.04.003.

811   Dolan, A.M., Haywood, A.M., Hunter, S.J., Tindall, J.C., Dowsett, H.J., Hill, D.J.,

812       Pickering, S.J., 2015. Modelling the enigmatic Late Pliocene Glacial Event –

813       Marine Isotope Stage M2, Global and Planetary Change 128, 47–60,

814       http://dx/doi.org/10.1016/j.gloplacha.2015.02.001.

815   Dowsett, H.J., Robinson, M.M., Haywood, A.M., Hill, D.J., Dolan, A.M.,

816       Stoll, D.K., Chan, W.-L., Abe-Ouchi, A., Chandler, M.A., Rosenbloom, N.A.,

817       Otto-Bliesner, B.L., Bragg, F.J., Lunt, D.J., Foley, K.M., Riesselman, C.R,

818       2012. An assessment of confidence in Pliocene global sea-surface

819       temperature, Nature Clim. Change 2, 365-371, doi:10.1038/nclimate1455.

820   Du, J., Haley, B.A., Mix, A.C., 2020. Evolution of the Global Overturning Circulation

821       since the Last Glacial Maximum based on marine authigenic neodymium

822       isotopes. QSR 241, 106396. https://doi.org/10.1016/j.quascirev.2020.106396.

823   Dwyer, G.S., Chandler, M.A., 2009. Mid- Pliocene sea level and continental ice

824       volume based on coupled benthic Mg/Ca palaeotemperatures and oxygen

825    isotopes, Philos. Trans. R. Soc. Ser. A, 367, 157–168, doi:10.1098/

826    rsta.2008.0222.

827 Expedition 306 Scientists, 2006. Site U1313. In: North Atlantic Climate, Proceedings

828    of the Integrated Ocean Drilling Program, 303/306,

829    http://dx.doi.org/10.2204/iodp.%20proc.303306.112.2006.

830 Farmer, J.R. et al., 2019. Deep Atlantic Ocean carbon storage and the rise of 100,000-

831    year glacial cycles. Nature Geosciences 12, 355-360.

832    https://doi.org/10.1038/s41561-019-0334-6.

833 Foster, G.L., Vance, D., Prytulak J., 2007. No change in the neodymium isotope

834    composition of deep water exported from the North Atlantic on glacial-

835    interglacial time scales. Geology 35(1). 37–40. doi:10.1130/G23204A.1.

836 Frank, M., Whiteley, N., Kasten, S., Hein, J.R., O'Nions, K., 2002. North Atlantic

837    deep water export to the Southern Ocean over the past 14 Myr: Evidence from

838    Nd and Pb isotopes in ferromanganese crusts. Paleoceanography 17, 12-11-12-

839    19. doi:10.1029/2000pa000606.

840 Gao, C., McAndrews, J.H., Wang, X., Menzies, J., Turton, C.L., Wood, B.D., Pei, J.,

841    Kodors, C., 2012. Glaciation of North America in the James Bay Lowland,

842    Canada, 3.5 Ma, Geology 40(11), 975–978, doi:10.1130/G33092.1

843 Garzoli, S.L., Dong, S., Fine, R., Meinen, C.S., Perez, R.C., Schmid, C., von Sebille,

844    E., Yao, Q., 2015. The fate of the Deep Western Boundary Current in the South

845    Atlantic. Deep-Sea Research I 103, 125–136.

846 Gu, S., Liu, Z., Jahn, A., Rempfer, J., Zhang, J., Joos, F., 2019. Modelling

847    neodymium isotopes in the ocean component of the Community Earth System

848    Model (CESM1). Journal of Advances in Modeling Earth Systems 11(3) 624-

849    640. Doi:10.1029/2018MS001538.

850   Haug, G.H., Tiedemann, R., 1998. Effect of the formation of the Isthmus of

851        Panama on Atlantic Ocean thermohaline circulation, Nature 393, 673–676.

852   Haywood, A.M., et al., 2013. On the identification of a Pliocene time slice for data-

853        model comparison. Philos. Trans. A Math. Phys. Eng. Sci. 371(2001):

854        20120515. doi:10.1098/rsta/2012.0515.

855   Hillaire-Marcel, C., de Vernal, A., Bilodeau, G., Weaver, A.J., 2001a. Absence of

856        deep-water formation in the Labrador Sea during the last interglacial period.

857        Nature 410, 1073–1077. https://doi.org/10.1038/35074059.

858   Hillaire-Marcel, C., de Vernal, A., Candon, L., Bilodeau, G., Stoner, J., 2001b.

859        Changes of Potential Density Gradients in the Northwestern North Atlantic

860        During the Last Climatic Cycle Based on a Multiproxy Approach. in The

861        Oceans and Rapid Climate Change: Past, Present, and Future. Geophys.

862        Monogr., 126, edited by D. Seidov, B. J. Haupt, and M. Maslin, pp. 83–100,

863        AGU, Washington, D. C. https://doi.org/10.1029/GM126p0083.

864   Hodell, D.A., Venz, K.A., 1992. Toward a high-resolution stable

865        isotopic record of the Southern Ocean during the Pliocene-Pleistocene (4.8 to

866        0.8 Ma), Antarctic Research Series 56, 265–310.

867   Hodell, D.A., Venz-Curtis, K.A., 2006. Late Neogene history of deepwater ventilation

868        in the Southern Ocean. Geochem. Geophys. Geosyste. 7, Q09001.

869   Howe, J.N.W., Piotrowski, A.M., Noble, T.L., Mulitza, S., Chiessi, C.M., Bayon, G.,

870        2016. North Atlantic Deep Water Production during the Last Glacial

871        Maximum. Nature Communications 7, 11765. doi:10.1038/ncoms11765.

872   Hu, R., Noble, T.L., Piotrowski, A.M., McCave, I.N., Bostock, H.C., Neil, H.L.,

873        2016. Neodymium isotopic evidence for linked changes in Southeast Atlantic

874      and Southwest Pacific circulation over the last 200 kyr. Earth Planet. Sci. Lett.

875      455, 106–114. https://doi.org/10.1016/j.epsl.2016.09.027.

876    Huang, H., Gutjahr, M., Eisenhauer, A., and Kuhn, G., 2020. No detectable Weddell

877      Sea Antarctic Bottom Water export during the Last and Penultimate Glacial

878      Maximum: Nature Communications 11, 424, https://doi.org/10.1038/ s41467-

879      020-14302-3.

880    Jansen, E., Fronval, T., Rack, F., Channell, J.E.T., 2000. Pliocene-Pleistocene ice

881      rafting history and cyclicity in the Nordic Seas during the last 3.5 Myr,

882      Paleoceanography 15(6), 709–721.

883    Jeandel, C., 1993. Concentration and isotopic composition of Nd in the South Atlantic

884      Ocean. EPSL 117(3–4), 581–591. https://doi.org/10.1016/0012-821(93)90104-

885      H.

886    Keigwin, L.D., 1987. Pliocene stable-isotope record of Deep Sea Drilling Project Site

887      606: Sequential events of $^{18}$O enrichment beginning at 3.1 Ma, Initial Rep.

888      Deep Sea Drill. Proj., 94, 911–920.

889    Kerr, J., Rickaby, R., Yu, J., Elderfield, H., Sadekov, A.Y., 2017. The effect of ocean

890      alkalinity and carbon transfer on deep-sea carbonate ion concentration during

891      the past five glacial cycles. EPSL 471, 42–53.

892    Kostov, Y., Armour, K.C., Marshall, J., 2014. Impact of the Atlantic meridional

893      overturning circulation on ocean heat storage and transient climate change.

894      Geophys. Res. Lett., 41(6), 2108–2116.

895    Lambeck, K., Rouby, H., Purcell, A., Sun, Y., Sambridge, M., 2014. Sea level and

896      global ice volumes from the Last Glacial Maximum to the Holocene. PNAS

897      111 (43) 15296-15303. https://doi.org/10.1073/pnas.1411762111.

898    Lambelet, M., van de Flierdt, T., Crocket, K., Rehkämper, M., Kreissig, K., Coles, B.,

899        Rijkenberg, M.J.A., Gerringa, L.J.A., de Baar, H.J.W., Steinfeldt, R., 2016.

900           Neodymium isotopic composition and concentration in the western North

901           Atlantic Ocean: results from the GEOTRACES GA02 section. Geochim.

902           Cosmochim. Acta 177, 1–29. http://dx. doi.org/10.1016/j.gca.2015.12.019.

903    Lang, D.C., Bailey, I., Wilson, P.A., Chalk, T.B., Foster, G.L., Gutjahr, M., 2016.

904           Incursions of southern-sourced water into the deep North Atlantic during late

905           Pliocene glacial intensification. Nature Geoscience volume 9, 375–379.

906           https://doi.org/10.1038/ngeo2688.

907    Lang, D.C., Bailey, I., Wilson, P.A., Beer, C., Bolton, C.T., Newsam, C.,

908           Spencer, M.R., Friedrich, O., Gutjahr, M., Foster, G.L., Cooper, C.J., Milton,

909           A., 2014. The transition on North America from the warm humid Pliocene to the

910           glaciated Quaternary traced by eolian dust deposition at a benchmark North

911           Atlantic Ocean drill site, Quaternary Science Reviews 93C, 125–141.

912           doi:10.1016/j.quascirev.2014.04.005.

913    Laskar, J. et al., 2004. A long-term numerical solution for the insolation quantities

914           of the Earth. A & A, 428. 261–285

915    Lauvset, S.K., Key, R.M., Olsen, A., van Heuven, S., Velo, A., Lin, X., Schirnick, C.,

916           Kozyr, A., Tanhua, T., Hoppema, M., 2016. A new global interior ocean

917           mapped climatology: the $1° \times 1°$ GLODAP version 2. Earth System Science

918           Data Discussions 8, 325–340.

919    Lawrence, K.T., Herbert, T.D., Brown, C.M., Raymo, M.E., and Haywood, A.M.,

920           2009. High-amplitude variations in North Atlantic sea surface temperature

921           during the early Pliocene warm Period, Paleoceanography 24, PA2218,

922           doi:10.1029/2008PA001669.

923    Lippold, J., Gutjahr, M., Blaser, P., Christner, E., de Carvalho Ferreira,. M.L.,

924     Mulitza, S., Christl, M., Frank Wombacher, F., Böhm, E., Antz, B.,

925     Cartapanis, O., Vogel, H., Jaccard, S.L., 2016. Deep water provenance and

926     dynamics of the (de)glacial Atlantic meridional overturning circulation. EPSL

927     445. 68–78. http://dx.doi.org/10.1016/j.epsl.2016.04.013.

928     Lisiecki, L.E., Raymo, M.E., 2005. A Pliocene–Pleistocene stack of 57 globally

929     distributed benthic delta-$^{18}$O records. Paleoceanography 20, PA1003,

930     http://dx.doi.org/10.1029/2005PA001164.

931     MacLeod, K.G., Martin, E.E., Blair, S.W., 2008. Nd isotopic excursion across

932     Cretaceous ocean anoxic event 2 (Cenomanian-Turonian) in the tropical North

933     Atlantic. Geology 36, 811–814. doi:10.1130/G24999a.1

934     Martin, E.E., Blair, S.W., Kamenov, G.D., Scher, H.D., Bourbon, E., Basak, C.,

935     Newkirk, D.N., 2010. Extraction of Nd isotopes from bulk deep sea sediments

936     for paleoceanographic studies on Cenozoic time scales. Chem. Geol. 269, 414-

937     431.

938     Martin, E.E., Scher, H.D., 2004. Preservation of seawater Sr and Nd isotopes in fossil

939     fish teeth: bad news and good news. Earth Planet. Sci. Lett. 220, 25–39.

940     Martínez-Botí, M.A., Foster, G.L, Chalk, T.B., Rohling, E.J., Sexton, P.F., Lunt, D.J.,

941     Pancost, R.D., Badger, M.P.S., Schmidt, D.N., 2015. Plio-Pleistocene climate

942     sensitivity evaluated using high-resolution CO2 records. Nature 518, 49–54.

943     http:// dx.doi.org/10.1038/nature14145.

944     Maslin, M.A., Li, X. S., Loutre, M.–F., Berger, A., 1998. The contribution of orbital

945     forcing to the progressive intensification of northern hemisphere glaciation,

946     Quat. Sci. Rev., 17, 411–426.

947     McCartney, M.S., Bennett, S.L., Woodgate-Jones, M.E., 1991. Eastward Flow

948     through the Mid-Atlantic Ridge at 11°N and Its Influence on the Abyss of the

949        Eastern Basin. Journal of Physical Oceanography 21, 1089–1121.

950    McCartney, M.S., 1992. Recirculating components to the deep boundary current of

951        the northern North Atlantic. Prog. Oceanog. 29, 283–383.

952    McClymont, E.L., Ford, H.L., Ho, S.L., Tindall, J.C., Haywood, A.M., Alonso-

953        Garcia, M., Bailey, I., Berke, M.A., Littler, K., Patterson, M.O., Petrick, B.,

954        Peterse, F., Ravelo, A.C., Risebrobakken, B., De Schepper, S., Swann, G.E.A.,

955        Thirumalai, K., Tierney, J.E., van der Weijst, C., White, S., Abe-Ouchi, A.,

956        Baatsen, M.L.J., Brady, E.C., Chan, W.-L., Chandan, D., Feng, R., Guo, C.,

957        von der Heydt, A.S., Hunter, S., Li, X., Lohmann, G., Nisancioglu, K.H.,

958        Otto-Bliesner, B.L., Peltier, W.R., Stepanek, C., Zhang, Z., 2020. Lessons

959        from a high-$CO_2$ world: an ocean view from $\sim$ 3 million years ago. Clim. Past

960        16, 1599–1615. https://doi.org/10.5194/cp-16-1599-2020.

961    McDonagh, E.L., Arhan, M., Heywood, K.J., 2002. On the circulation of bottom

962        water in the region of the Vema Channel. Deep-Sea Research I 49, 1119–

963        1139.

964    McKay, R., et al., 2012. Antarctic and Southern Ocean influences on Late Pliocene

965        global cooling. PNAS 109(17), 6423–6428. doi:10.1073/PNAS/1112248109.

966    Mercier, H., Morin, P., 1997. Hydrography of the Romanche and Chain Fracture

967        Zones. Journal of Geophysical Research 102(C5), 10373–10389.

968    Mercier, H., Weatherly, G.L., Arhan, M., 2000. Bottom water throughflows at the rio

969        de Janeiro and Rio Grande Fracture Zones. GRL 27(10), 1503–1506.

970    Meredith, M.P., Jullion, L., Brown, P.J., Naveira Garabato, A.C., Couldrey, M.P.,

971        2014. Dense waters of the Weddell and Scotia Seas: recent changes in

972        propertiesand circulation. Philosophical Transactions of the Royal Society A

973        372 (2019) https://doi.org/10.1098/rsta.2013.0041.

974  Miller, K.G., Wright, J.D., Browning, J.V., Kulpecz, A.A., Kominz, M.A.,

975      Naish, T.R., Cramer, B.S., Rosenthal, Y., Peltier, R.W., Sosdian, S., 2012. The

976      high tide of the warm Pliocene: Implications of global sea level for Antarctic

977      deglaciation, Geology, 40, 407–410.

978  Mix, A.C., Pisias, N. G., Rugh, W., Wilson, J., Morey, A., Hagelberg, T.K., 1995.

979      Benthic foraminfer stable isotope record from Site 849 (0-5 Ma): local and

980      global climate changes. *Procs*. *Ocean Drill*. *Prog*, *Sci*. *Res*. 138, 371–412.

981  Mudelsee, M., Raymo, M.E., 2005. Slow dynamics of the northern hemisphere

982      glaciation. Paleoceanography 20, PA4022.

983      http://dx.doi.org/10.1029/2005PA001153.

984  Naafs, B.D.A., Ruediger, S.R., Hefter, J., Khelifi, N., De Schepper, S., Haug, G.H.,

985      2010. Late Pliocene changes in the North Atlantic Current, EPSL 298, 434–442.

986      https://doi.org/10.1016/j.epsl.2010.08.023.

987  Naafs, B.D.A., Hefter, J., Stein, R., 2014. Millennial-scale ice rafting events and

988      Hudson Strait Heinrich(-like) Events during the late Pliocene and Pleistocene: a

989      review. QSR 80, 1-28. http://dx.doi.org/10.1016/j.quascirev.2013.08.014.

990  Naafs, B.D.A., Voelker, A.H.L., Karas, C., Andersen, N., Sierro, F.J., 2020. Repeated

991      near-collapse of the Pliocene sea surface temperature gradient in the North

992      Atlantic. Paleoceanography and Paleoclimatology, 35(5),

993      doi:10.1029/2020PA003905.

994  Naish, T., 1997. Constraints on the amplitude of late Pliocene eustatic sea level

995      fluctuations: new evidence from the New Zealand shallow marine sediment

996      record. Geology 25 (12), 1139–1142, http://dx.doi.org/10.1130/0091-

997      7613(1997)025 < 1139:COTAOL > 2.3.CO;2.

998  Naish, et al., 2009. Obliquity-paced Pliocene West Antarctic ice sheet oscillations.

999          Nature 458, 322–328. https://doi.org/10.1038/nature07867.

1000    Ng, H.C., Robinson, L.F., McManus, J.F., Mohamed, K.J., Jacobel, A.W., Ivanovic,

1001          R.F., Gregoire, L.J., Chen, T., 2018. Coherent deglacia changes in western

1002          Atlantic Ocean circulation. Nature Communications 9, 2947, https://

1003          doi.org/10.1038/s41467-018-05312-3.

1004    Nikurashin, M., Vallis, G., 2011. A Theory of Deep Stratification and Overturning

1005          Circulation in the Ocean, J. Phys. Oceanogr. 41(3), 485–502,

1006          doi:10.1175/2010JPO4529.1.

1007    O'Nions, R.K., Frank, M., von Blanckenburg, F., Ling, H.F., 1998. Secular variation

1008          of Nd and Pb isotopes in ferromanganese crusts from the Atlantic, Indian and

1009          Pacific Oceans. EPSL 155, 15–28. doi:10.1016/S0012-821x(97)00207-0.

1010    Oppo, D.W., Raymo, M.E., Lohmann, G.P., Mix, A.C., Wright, J.D., Prell, W.L.,

1011          1995. A $\delta^{13}C$ record of Upper North Atlantic Deep Water during the past 2.6

1012          million years. Paleoceanog. 10(3), 373-394.

1013    Oppo, D.W., Fairbanks, R.G., 1987. Variability in the deep and intermediate water

1014          circulation of the Atlantic Ocean: Northern hemisphere modulation of the

1015          Southern Ocean, EPS, 86, 1–15.

1016    Patterson, M.O., McKay, R., Naish, T., Bostock, H. C., Dunbar, R., Ohneiser, C., et

1017          al., 2018. A southwest Pacific perspective on long-term global trends in

1018          Pliocene-Pleistocene stable isotope records. Paleoceanography and

1019          Paleoclimatology 33, 825–839. https:// doi.org/10.1029/2017PA003269.

1020    Pena, L.D., Goldstein, S., 2014. Thermohaline circulation crisis and impacts during

1021          the mid-Pleistocene transition. Science 345 (6194).

1022          Doi:10.1126/science/1249770.

1023    Piotrowski, A.M., Goldstein, S.L., Hemming, S.R., Fairbanks, R.G., 2005. Temporal

relationships of carbon cycling and ocean circulation at glacial boundaries.

Science 307, 1933–1938, doi:10.1126/Science.1104883.

Pöppelmeier, F., Gutjahr, M., Blaser, P., Keigwin, L.D., Lippold, J., 2018. Origin of

abyssal water mass in the NW Atlantic since the Last Glacial Maximum.

Paleoceanogr. Paleoclimatol. 33 (5), 530–543.

https://doi.org/10.1029/2017PA003290.

Pöppelmeier, F., Blaser, P., Gutjahr, M., Süfke, F., Thornalley, D.J.R., Grützner, J.,

Jakob, K.A., Link, J.M., Szidat, S., Lippold, J., 2019a. Influence of ocean

circulation and benthic exchange on deep Northwest Atlantic Nd isotope

records during the past 30,000 years. Geochem. Geophys. Geosyst. 20, 4457–

4469. https://doi.org/ 10.1029/2019GC008271.

Pöppelmeier, F., Gutjahr, M., Blaser, P., Oppo, D.W., Jaccard, S.L., Regelous, M.,

Huang, K.-F., Süfke, F., Lippold, J., 2019b. Water mass gradients of the mid-

depth Southwest Atlantic during the past 25,000 years. EPSL 531, 115963.

https://doi.org/10.1016/j.epsl.2019.115963.

Pöppelmeier, F., Gutjahr, M., Blaser, P., Jaccard, S.L., Frank, M., Max, L., Lippold,

J., 2020. Northern-sourced water dominated the Atlantic Ocean during the

Last Glacial Maximum. Geology 48. https:// doi.org/10.1130/G47628.1.

Prell, W.L., 1984. Covariance patterns of foraminiferal $\delta^{18}$O: An evaluation of

Pliocene ice volume changes near 3.2 million years ago, Science, 226, 692–

694, doi:10.1126/ science.226.4675.692.

Rae, J.W., Foster, G.L., Schmidt, D.N., Elliott, T., 2011. Boron isotopes and B/Ca in

benthic foraminifera: Proxies for the deep ocean carbonate system. Earth and

Planetary Science Letters 302, 403-413.

Raymo, M.E., Ruddiman, W.F., Clement, B.M., 1987. Pliocene/Pleistocene

1049      paleoceanography of the North Atlantic at DSDP Site 609. Initial Reports of the

1050      Deep Sea Drilling Project, v.94, p. 895-901.

1051    Raymo, M.E., Ruddiman, W.F., Shackleton, N.J., Oppo, D.W., 1990. Evolution of

1052      the Atlantic-Pacific d$^{13}$C gradients over the last 2.5 m.y., EPSL 97, 353–368.

1053    Raymo, M.E., Hodell, D., Jansen, E., 1992. Response of deep ocean circulation to the

1054      initiation of northern hemisphere glaciation (3-2 M.Y.), Paleoceanography, 7,

1055      645–672.

1056    Raymo, M.E., Oppo, D.W., Flower, B.P., Hodell, D.A., McManus, J.F., Venz, K.A.,

1057      Kleiven, K.F., McIntyre, K., 2004. Stability of North Atlantic water masses in

1058      face of pronounced climate variability during the Pleistocene.

1059      Paleoceanography 19(2), PA2008, doi:10.1029/2003PA000921.

1060    Reynolds, B., Frank, M., O'Nions, R., 1999. Nd-and Pb-isotope time series from

1061      Atlantic ferromanganese crusts: implications for changes in provenance and

1062      paleocirculation over the last 8 Myr. *Earth and Planetary Science Letters* **173**,

1063      381-396, doi:10.1016/S0012-821X(99)00243-5.

1064    Reynolds, B.C., Sherlock, S.C., Kelley, S.P., Burton, K.W., 2004. Radiogenic isotope

1065      records of Quaternary glaciations: Changes in the erosional source and

1066      weathering processes. Geology 32(10), 861-864. Doi:10.1130/G20734.1.

1067    Roberts, N.L., Piotrowski, A.M., 2015. Radiogenic Nd isotope labeling of the

1068      northern NE Atlantic during MIS 2. Earth and Planetary Science Letters 423,

1069      125–133. https://doi.org/10.1016/j.epsl.2015.05.011.

1070    Ruddiman, W.F., M.E. Raymo, D.G. Martinson, B.M. Clement, and J. Backman,

1071      1989, Mid-Pleistocene evolution of Northern Hemisphere climate.

1072      Paleoceanography 4, 353-412.

1073    Sandoval, F.J., Weatherly, G.L., 2000. Evolution of the Deep Western Current of

1074          Antarctic Bottom Water in the Brazil Basin. Journal of Physical

1075          Oceanography 31, 1140–1460.

1076     Sarnthein, M., Winn, K., Jung, S.J.A., Duplessy, J.-C., Labeyrie, L., Erlenkeuser, H.,

1077          Ganssen, G., 1994. Changes in East Atlantic deepwater circulation over the

1078          last 30,000 years: eight time slice reconstructions. Paleoceanography 9, 209–

1079          267. https://doi.org/10.1029/93PA03301.

1080     Schlitzer, R., 2002. Interactive analysis and visualization of geoscience data with

1081          Ocean Data View. *Computers & Geosciences* 28, 1211–1218,

1082          doi:10.1016/S0098-3004(02)00040-7.

1083      Seki, O., Foster, G.L., Schmidt, D.N., Mackensen, A., Kawamura, K., Pancost, R.D.,

1084          2010. Alkenone and boron-based Pliocene pCO2 records, Earth Planet. Sci.

1085          Lett. 292, 201–211. https://doi.org/10.1016/j.epsl.2010.01.037.

1086     Shackleton, N.J., Hall, M.A., Vincent, E., 2000. Phase relationships between

1087          millennial-scale events 64,000-24,000 years ago. Paleoceanography 15(6), 565–

1088          569. https://doi.org/10.1029/2000PA000513.

1089     Smyth-Wright, D., Boswell, S., 1998. Abyssal circulation in the Argentine Basin.

1090          Journal of Geophysical Research 103(C8), 15845–15851.

1091     Stephens, J.C., Marshall, D.P., 2000. Dynamical Pathways of Antarctic Bottom Water

1092          in the Atlantic. Journal of physical Oceanography 30, 622–640.

1093     Stichel, T., Frank, M., Rickli, J., Haley, B.A., 2012. The hafnium and neodymium

1094          isotope composition of seawater in the Atlantic sector of the Southern Ocean.

1095          Earth Planet. Sci. Lett. 317, 282–294.

1096     Stramma, L., England, M., 1999. On the water masses and mean circulation of the

1097          South Atlantic Ocean. Journal of Geophysical Research 104, C9, 20863–20883.

1098     Tan, N., Ramstein, G., Dumas, C., Contoux, C., Ladant, J.-B., Sepulchre, P., Zhang,

1099       Z., De Schepper, S., 2017. Exploring the MIS M2 glaciation occurring during a

1100       warm and high atmospheric CO2 Pliocene background climate. Earth and

1101       Planetary Science Letters 472, 266–276.

1102  Tanaka, T., Togashi, S., Kamioka, H., Amakawa, H., Kagami, H., Hamamoto, T.,

1103       Yuhara, M., Orihashi, Y., Yoneda, S., Shimizu, H., Kunimaru, T., Takahashi,

1104       K., Yanagi, T., Nakano, T., Fujimaki, H., Shinjo, R., Asahara, Y., Tanimizu, M.,

1105       Dragusanu, C., 2000. JNdi-1: a neodymium isotopic reference in consistency

1106       with LaJolla neodymium. Chemical Geology 168, 279–281. doi:10.1016/S0009-

1107       2541(00)00198-4.

1108  Vance, D., Burton, K., 1999. Neodymium isotopes in planktonic foraminifera:

1109       a record of the response of continental weathering and ocean circulation rates to

1110       climate change. EPSL 173, 365-379.

1111  Vance, D., Thirlwall, M., 2002. An assessment of mass discrimination in MC-ICPMS

1112       using Nd isotopes. Chemical Geology 185, 227-240. 10.1016/S0009-

1113       2541(01)00402-8.

1114  Venz, K.A., Hodell, D.A., Stanton, C., Warnke, D.A., 1999. A 1.0 Myr record of

1115       glacial North Atlantic intermediate water variability from ODP site 982 in the

1116       northeast Atlantic. Paleoceanography 14, 42-52, doi:10.1029/1998pa900013.

1117  Venz, K.A., Hodell, D.A., 2002. New evidence for changes in Plio–Pleistocene deep

1118       water circulation from Southern Ocean ODP Leg 177 Site 1090.

1119       Palaeogeography, Palaeoclimatology, Palaeoecology 182, 197–220,

1120       doi:10.1016/S0031-0182(01)00496-5.

1121  Wienders, N., Arhan, M., Mercier, H., 2000. Circulation at the western boundary of

1122       the South and Equatorial Atlantic: Exchanges with the ocean interior. Journal of

1123       Marine Research 58, 1007–1039.

1124 Wilson, D.J., Crocket, K.C., van de Flierdt, T., Robinson, L.F. & Adkins, J.F., 2014.

1125    Dynamic intermediate ocean circulation in the North Atlantic during Heinrich

1126    Stadial 1: A radiocarbon and neodymium isotope perspective,

1127    Paleoceanography 29, 1072–1093.

1128 Yu, J.M., Elderfield, H., 2007. Benthic foraminiferal B/Ca ratios reflect deep water

1129    carbonate saturation state. Earth and Planetary Science Letters, 73-86.

1130 Yu, J., Elderfield, H., Piotrowski, A.M., 2008. Seawater carbonate ion-delta C-13

1131    systematics and application to glacial-interglacial North Atlantic ocean

1132    circulation. Earth and Planetary Science Letters 271, 209-220.

1133 Yu, J., Anderson, R.F., Jin, Z., Menviel, L., Zhang, F., Ryerson, F.J., Rohling, E.J.,

1134    2014. Deep South Atlantic carbonate chemistry and increased interocean deep

1135    water exchange during last deglaciation. Quat. Sci. Rev. 90, 80–89.

1136 Zhao, N., Oppo, D.W., Huang, K. et al., 2019. Glacial–interglacial Nd isotope

1137    variability of North Atlantic Deep Water modulated by North American ice

1138    sheet. *Nat Commun*. 10, 5773. https://doi.org/10.1038/s41467-019-13707-z.

1139

1140 **Figure Captions**

1141 **Figure 1.** Climate indicators across marine isotope stage (MIS) M2, ~3.3 Ma, and the

1142 Plio-Pleistocene intensification of northern hemisphere glaciation, ~3.5-2.5 Ma

1143 (Mudelsee and Raymo, 2005): **(A)** Site U1313 $\varepsilon_{Nd}$ composition of fish debris (Lang et

1144 al., 2016). Estimates of the $\varepsilon_{Nd}$ composition of Northern Component Water, NCW,

1145 (red bar) follow Lang et al. (2016) and is taken as the average value of Fe-Mn crust

1146 $\varepsilon_{Nd}$ (and their 2 s.d.) from TR079-D14 (Reynolds et al., 1999), BM1969.05 (Burton et

1147 al., 1997; 1999; on chronology of O'Nions et al., 1998), ALV539 2-1 (Burton et al,

1148 1999; on chronology of O'Nions et al., 1998) spanning 2.4-3.3 Ma. Estimate for

1149    Southern Component Water, SCW, (blue bar) is average value of Fe-Mn crust $\varepsilon_{Nd}$

1150    (and their 2 s.d.) from D18-1 (Frank et al., 2002) spanning 2.4-3.3 Ma; **(B)** Site

1151    U1313 (Lang et al., 2014), Site 1267 (Bell et al., 2014) and ODP Site 982 (Hodell and

1152    Venz-Curtis, 2006) benthic $\delta^{13}$C; **(C)** a stack of globally representative benthic $\delta^{18}$O

1153    records, the LR04 (grey; Lisiecki and Raymo, 2005) and benthic $\delta^{18}$O from North

1154    Atlantic Ocean IODP Site U1313 (black; Bolton et al., 2010) and Walvis Ridge (red;

1155    Bell et al., 2014). The mid Piacenzian warm period (mPWP) is labelled. The

1156    black/white bar at the bottom of the figure denotes palaeomagnetic (sub)chronozones

1157    (Cande and Kent, 1995); M = Matuyama, G = Gauss, K = Keana and Ma =

1158    Mammoth. See Figure 2 and Supplementary Figure S1 for site locations.

1159

1160    **Figure 2.** Location of Atlantic Ocean drill sites used in this study (Sites 1267 and

1161    U1313, red circles) and others (black circles) discussed in the main text. Also shown

1162    is a schematic of modern pathways of deep-waters relevant to our study sites: NADW

1163    = North Atlantic Deep Water (dark grey lines), AABW = Antarctic Bottom Water

1164    (light blue lines), LSW = Labrador Sea Water, DSOW = Denmark Strait Overflow

1165    Water, ISOW = Iceland Scotland Overflow Water (ISOW), WTRO = Wyville

1166    Thomson Ridge Overflow, NGS = Norwegian Greenland Seas. The Verma (VFZ),

1167    Romanche (RGZ), Chain (CFZ), Rio de Janeiro (RJFZ) and Rio Grande (RGFZ)

1168    fracture zones and Walvis Passage (WP) are also labelled and represent important

1169    pathways for AABW to the eastern Atlantic (see main text). The Kane Gap (GP) is

1170    also labelled. Depths stated for VFZ, RGZ, RJFZ and RGFZ are known maximum

1171    depths through which SCW can pass through these fracture zones. Bottom-water

1172    pathway reconstructions based on: McCartney et al. (1991); McCartney (1992); Coles

1173    et al. (1996); Smyth-Wright and Boswell (1998); Stramma and England (1999);

1174    Wienders et al. (2000); Sandoval and Weatherly (2000); Choboter and Swaters

1175    (2000); Mercier et al. (2000); Stephens and Marshall (2000); McDonagh et al. (2002);

1176    Arhan et al. (2003); Meredith et al. (2014); Garzoli et al. (2015).

1177

1178    **Figure 3.** Water-mass provenance tracers from ODP Site 1267 (red) and IODP Site

1179    U1313 for the last glacial-Holocene, MIS 100 and MIS M2. (A-C) fresh volcanic

1180    glass per gram of dry sediment at Site U1313. Last glacial volcanic glass data in A is

1181    from Lang et al. (2016). MIS 100 and MIS M2 volcanic glass data in B and C were

1182    generated in this study; (D-F) benthic B/Ca data from Site 1267; (G-I) fish debris Nd

1183    isotope data ($\varepsilon_{Nd}$) from sites 1267 and U1313; (J-L) benthic $\delta^{13}C$ and (M-O) benthic

1184    $\delta^{18}O$ data from sites 1267 and U1313. Error bars (2 s.d.) for stable isotope data

1185    reported by Bolton et al. (2010) for Site U1313 (benthic $\delta^{18}O$ = 0.065‰; benthic $\delta^{13}C$

1186    = 0.031‰), by Bell et al. (2014) for Site 1267 (benthic $\delta^{18}O$ and $\delta^{13}C$ = < 0.1‰) and

1187    by Chalk et al. (2019) for Site U1313 (benthic $\delta^{18}O$ = 0.08‰; benthic $\delta^{13}C$ = 0.02‰)

1188    are not shown. See Figure 2 for site locations.

1189

1190    **Figure 4.** Comparison of water-mass provenance tracers predominantly from the

1191    Atlantic Ocean for the last glacial-Holocene, MIS 100 and MIS M2: (A-C) $[CO_3^{2-}]$

1192    estimates based on benthic B/Ca data; (D-F) fish debris Nd isotope data ($\varepsilon_{Nd}$) from

1193    sites 1267 and U1313 alongside estimates of the $\varepsilon_{Nd}$ composition of Northern

1194    Component Water (NCW) and the Southern Component Water (SCW) end-members.

1195    NCW for MIS M2 and MIS 100 is estimated following Lang et al. (2016) and is taken

1196    as the average value of Fe-Mn crust $\varepsilon_{Nd}$ (and their 2 s.d.) from TR079-D14 (Reynolds

1197    et al., 1999), BM1969.05 (Burton et al., 1997; 1999; on chronology of O'Nions et al.,

1198    1998), ALV539 2-1 (Burton et al, 1999; on chronology of O'Nions et al., 1998)

1199    spanning 2.4-3.3 Ma. Also shown in (D) is a composite Nd isotope record from

1200    KNR198 from the New England Slope in the northwest North Atlantic, considered by

1201    Zhao et al. (2019) to record the evolution of NCW over the past ~21 ka. Estimate for

1202    the SCW end-member during MIS M2 and MIS 100 is average value of Fe-Mn crust

1203    $\varepsilon_{Nd}$ (and their 2 s.d.) from D18-1 (Frank et al., 2002) spanning 2.4-3.3 Ma. Last

1204    glacial-Holocene NADW defined as average (and their 2 s.d.) of Holocene U1313

1205    data (<14 ka; MIS 2/1 boundary as defined by Lisiecki and Raymo, 2005). Last

1206    glacial-Holocene SCW end-member estimated using an average value of Fe-Mn crust

1207    $\varepsilon_{Nd}$ (and their 2 s.d.) from D18-1 (Frank et al., 2002) spanning 0-0.04 Ma. Vertical

1208    range bars in D show range of modern Upper and Lower North Atlantic Deep Water

1209    (UNADW and LNADW, respectively) $\varepsilon_{Nd}$ (Lambelet et al., 2016); (G-I) fresh

1210    volcanic glass and ice-rafted debris (IRD) >150 μm per gram of dry sediment at Site

1211    U1313. Last glacial, MIS 100 and MIS M2 IRD data from Lang et al. (2014), Lang et

1212    al. (2016) and Bolton et al. (2010); (J-L) benthic $\delta^{13}C$ data (including estimates of the

1213    $\delta^{13}C$ of NCW and SCW); (M-O) benthic $\delta^{18}O$ data. Error bar shown for benthic $\delta^{13}C$

1214    ($\delta^{18}O$) signifies that the uncertainty for the different sources of these data plotted is no

1215    larger than 0.1 ‰ (0.15 ‰) at 2 s.d. See Figure 2 and Supplementary Figure S1 for

1216    site locations.

1217

1218    **Figure 5.** $\delta^{13}C$: [$CO_3^{2-}$] cross plot. B/Ca-derived carbonate data and co-occurring $\delta^{13}C$

1219    data from ODP Site 1267 for Marine Isotope Stage, MIS, 2-Holocene (A), and MIS

1220    99, 100, 101, M1, M2 and MG1 (B). Data from IODP U1313 (hollow green

1221    interglacial circles and solid green glacial circles; Chalk et al., 2019), IODP U1308

1222    (hollow black interglacial circles and solid black glacial circles; Chalk et al., 2019),

1223    ODP 980 (hollow light brown interglacial circles and solid light brown glacial circles;

1224    Chalk et al., 2019) are also shown in (A). Shown in both panels are shaded

1225    endmember compositions for the Southern Ocean (grey oval, Yu et al., 2014) and the

1226    Pacific (yellow oval, Kerr et al. (2017), based on Last Glacial Maximum and

1227    Holocene data from these regions. The Last Glacial Maximum northern (NADW)

1228    endmember is assumed to be denoted by the cluster of glacial ODP 980 points (solid

1229    light brown circles). Calculated slopes for $CO_2$ addition/evasion due to AABW-

1230    NADW mixing only (pale blue, dashed) and biological utilization (black, dashed) are

1231    shown. Sample gradients for alkalinity and temperature change are also shown,

1232    following Yu et al. (2008). See Figure 2 for site locations.

1233

1234    **Figure 6.** Palaeoceanographic proxies spanning marine isotope stage (MIS) M2, ~3.3

1235    Ma: (A) interpolated 1-kyr resolution $\delta^{11}B$-derived $CO_2$ data from *Globigerinoides*

1236    *ruber* white *sensu stricto* (with a 6-point running mean) at ODP Site 999 (Martinez-

1237    Boti et al., 2015; de la Vega et al., 2020). Shading = 68% (dark red) and 95% (light

1238    red) confidence intervals; (B) summer boreal (June 21st) and austral (December 21st)

1239    insolation forcing at 65˚N and 65˚S, respectively (Laskar, 2004); (C) Site U1313

1240    benthic $\delta^{13}C$ (Lang et al., 2014) and fish debris $\varepsilon_{Nd}$ (thus study; Lang et al., 2016) and

1241    estimates of the $\delta^{13}C$ of NCW (Site 982; Venz et al., 1999) and SCW (Site 849; Mix

1242    et al., 1995; Site 1123; Patterson et al., 2018) with data symbols removed for clarity;

1243    (D) Site 1267 benthic $\delta^{13}C$ (Lang et al., 2014) and fish debris $\varepsilon_{Nd}$ (thus study) and

1244    estimates of the $\delta^{13}C$ of NCW (Site 982; Venz et al., 1999) and SCW (Site 849; Mix

1245    et al., 1995; Site 1123; Patterson et al., 2018) with data symbols removed to aid

1246    plotting clarity; (E) $[CO_3^{2-}]$ estimates from Site 1267 based on benthic B/Ca data; (F)

1247    Benthic $\delta^{18}O$ data from Site U1313 (Bolton et al., 2010) and Site 1267 (this study).

1248    Horizontal dashed line in D represents atmospheric $CO_2$ value considered to be an

1249 important threshold for extensive glaciation of continents in the northern hemisphere

1250 (De Conto et al., 2008). All records plotted on LR04-based age models. See Figure 2

1251 and Supplementary Figure S1 for site locations.

1252

1253 **Figure 7.** Palaeoceanographic proxies spanning marine isotope stage (MIS) M2, ~3.3

1254 Ma and periods of early and late Pliocene warmth: (A) globally representative benthic

1255 $\delta^{18}O$ stack the LR04 (grey; Lisiecki and Raymo, 2005) and benthic $\delta^{18}O$ from North

1256 Atlantic Ocean IODP Site U1313 (black; Bolton et al., 2010); (B) fish debris Nd isotope

1257 data ($\epsilon_{Nd}$) from sites 1267 and U1313 alongside estimates of the $\epsilon_{Nd}$ composition of

1258 NCW and SCW water-mass end-member (see Figure 4 and main text for methods); (C)

1259 benthic $\delta^{13}C$ data from sites 1267 and U1313 and estimates of the $\delta^{13}C$ of Northern

1260 component waters (NCW) and southern component waters (SCW); (D) interpolated 1-

1261 kyr resolution $\delta^{11}B$-derived $CO_2$ data from *Globigerinoides ruber* white *sensu stricto*

1262 (with a 6-point running mean) at ODP Site 999 (Martinez-Boti et al., 2015; de la Vega

1263 et al., 2020). Shading = 68% (dark red) and 95% (light red) confidence intervals; (E)

1264 summer boreal (June 21st) and austral (December 21st) insolation forcing at 65˚N and

1265 65˚S, respectively (Laskar, 2004); (F) Alkenone-based reconstructions of sea-surface

1266 temperature (SST) from Nordic Seas ODP Hole 642B at 67˚N (Bachem et al., 2017),

1267 subpolar North Atlantic subpolar North Atlantic ODP Site 982 at 58˚N (Lawrence et

1268 al., 2009), DSDP Hole 610A at 53˚N (Naafs et al., 2020) and IODP Site U1313 at

1269 41˚N (Naafs et al., 2010); abundance of dinoflagellate cyst *Operculodinium*

1270 *centrocarpum* (De Schepper et al., 2009; De Schepper et al., 2013), with increased

1271 numbers taken to indicate the presence of the NAC over a study site (De Schepper et

1272 al., 2013), at (G) DSDP Site 610 and IODP Site U1308, and at (H) Site U1313 (De

1273 Schepper et al., 2013). All data plotted on LR04 or respective published age models.

1274    mPWP = mid Piacenzian Warm Period. Horizontal dashed line in D represents

1275    atmospheric $CO_2$ value considered to be an important threshold for extensive glaciation

1276    of continents in the northern hemisphere (DeConto et al., 2008). Colour-coded

1277    horizontal dashed lines in F are averages of equivalent Holocene-aged SST data from

1278    the same site. A modern SST value is highlighted for Hole 610A since no equivalent

1279    Holocene-aged alkenone SST data are available for this site. See Figure 2 and

1280    Supplementary Figure S1 for site locations.

1281

1282    **Figure 8.** Sub-polar North Atlantic dinoflagellate cyst records and their schematic

1283    interpretation in terms of North Atlantic Current (NAC) evolution during MIS M2:

1284    (Ai) abundance of dinoflagellate cyst *Operculodinium centrocarpum* (De Schepper et

1285    al., 2009; De Schepper et al., 2013), with increase numbers taken to indicate the

1286    presence of the NAC over a study site (De Schepper et al., 2013), at DSDP Site 610

1287    and IODP Site U1308, (Aii) and at Site U1313 (De Schepper et al., 2013). (Aii)

1288    Globally representative benthic $\delta^{18}O$ stack the LR04 (grey; Lisiecki and Raymo,

1289    2005) and benthic $\delta^{18}O$ from North Atlantic Ocean IODP Site U1313 (black; Bolton

1290    et al., 2010). Numbers 1-3 in (A) relate to NAC pathway interpretations illustrated in

1291    map shown in B-D. The most southerly position for the NAC during MIS M2 shown

1292    in map 2 is inferred from peak abundances of *O. centrocarpum* in U1313 sediments

1293    during early glacial conditions. A latitudinal position for the NAC in map 3 that is

1294    intermediate between the extremes shown in maps 1 and 2 is based on low

1295    abundances of *O. centrocarpum* in both U1313 and 610A/U1308 sediments during

1296    full glacial MIS M2.

1297

1298

1299    Table 1. Average values of water mass proxy data from Site 1267 (U1313) during

1300    target glacials (G) and associated interglacials (IG), as well as average IG-G change.

| | Marine Isotope Stage average* | | | | IG-G difference | | |
|---|---|---|---|---|---|---|---|
| **MIS** | $\varepsilon_{Nd}$ | $\delta^{13}C$ | $[CO_3^{2}]$ | | $\Delta\varepsilon_{Nd}$ | $\Delta\delta^{13}C$ | $\Delta[CO_3^{2}]$ |
| **MG1** | -11.03 (-11.92) | +0.85 (0.80) | 92.7 | **MG1-M2** | +1.09 (+0.70) | -0.46 (-0.20) | -0.5 |
| **M2** | -9.95 (-11.22) | +0.39 (0.59) | 92.1 | | | | |
| **M1** | -11.04 (-11.60) | +0.79 (0.83) | 103.1 | **M1-M2** | -1.10 (-0.37) | +0.40 (+0.23) | 11 |
| **101** | -11.18 (-12.55) | +0.55 (0.88) | 108.1 | **101-100** | -1.87 (+1.84) | -0.41 (-0.76) | 22.2 |
| **100** | -9.31 (-10.71) | +0.14 (0.12) | 85.8 | | | | |
| **99** | -10.04 (-11.88) | +0.30 (0.89) | 102.1 | **99-100** | -0.73 (-1.17) | +0.16 (+0.76) | 16.2 |
| **MIS 2** | -9.57 (-11.48) | +0.05 (0.19) | 82.3 | | | | |
| **MIS 1** | -10.74 (-13.98) | +0.57 (0.90) | 92.9 | **1-2** | -1.17 (-1.84) | +0.52 (+0.55) | 10.6 |

1301    *determined using LR04 definitions of MIS boundaries (Lisiecki and Raymo, 2005) apart from for

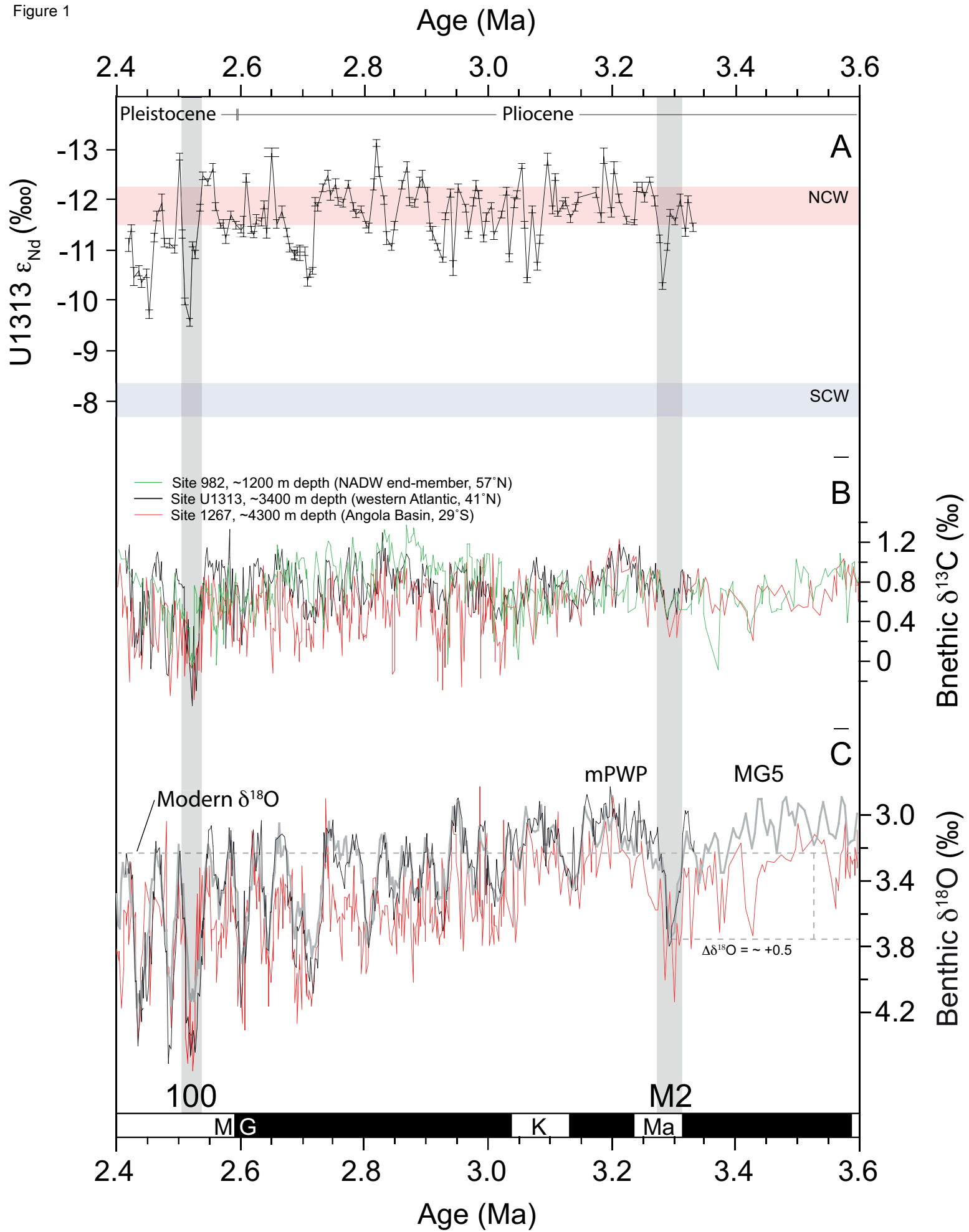1302    MIS M1 (where we use 3238-3285 ka) and MIS M2 (where we use 3285-3312 ka).
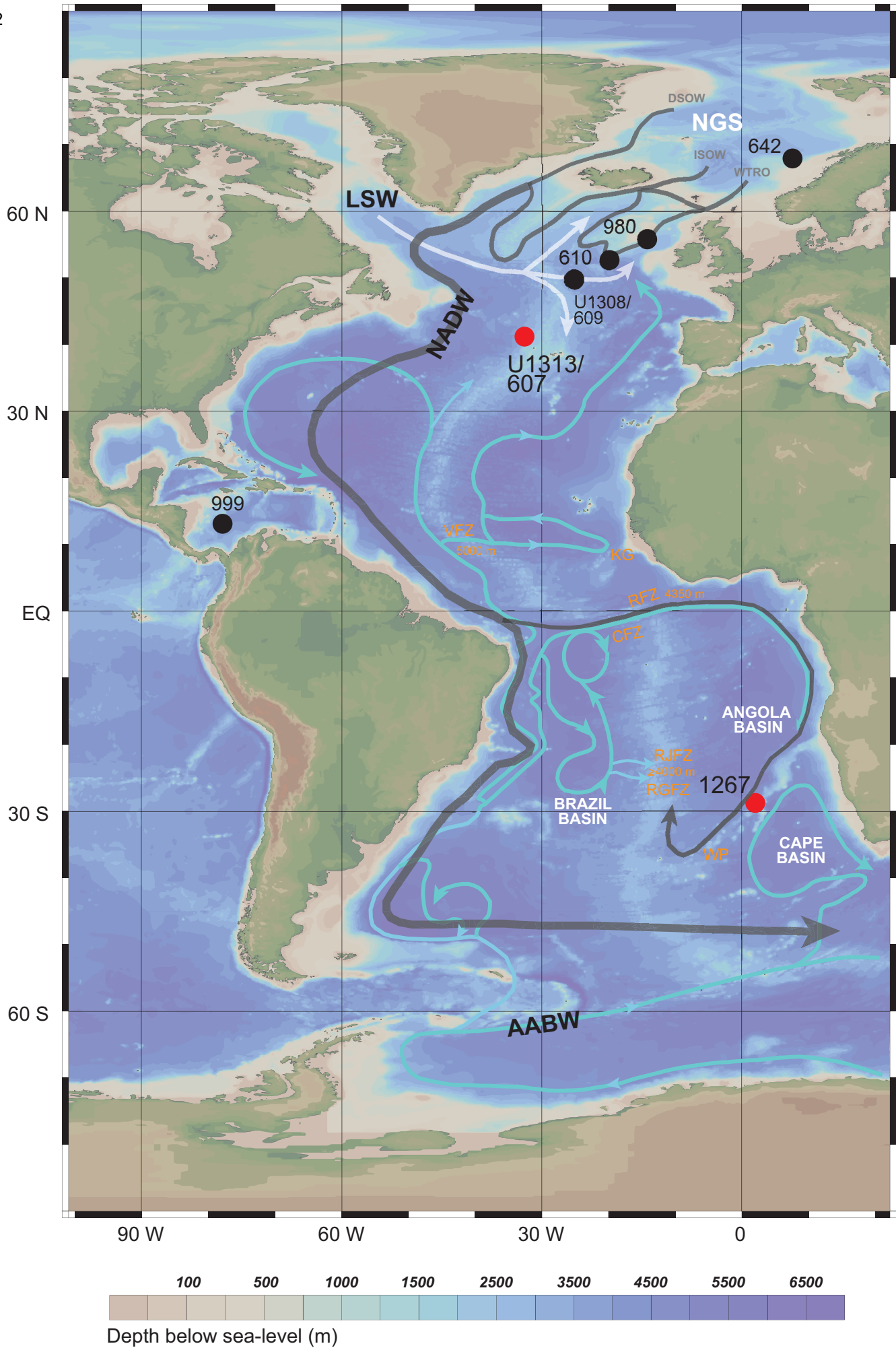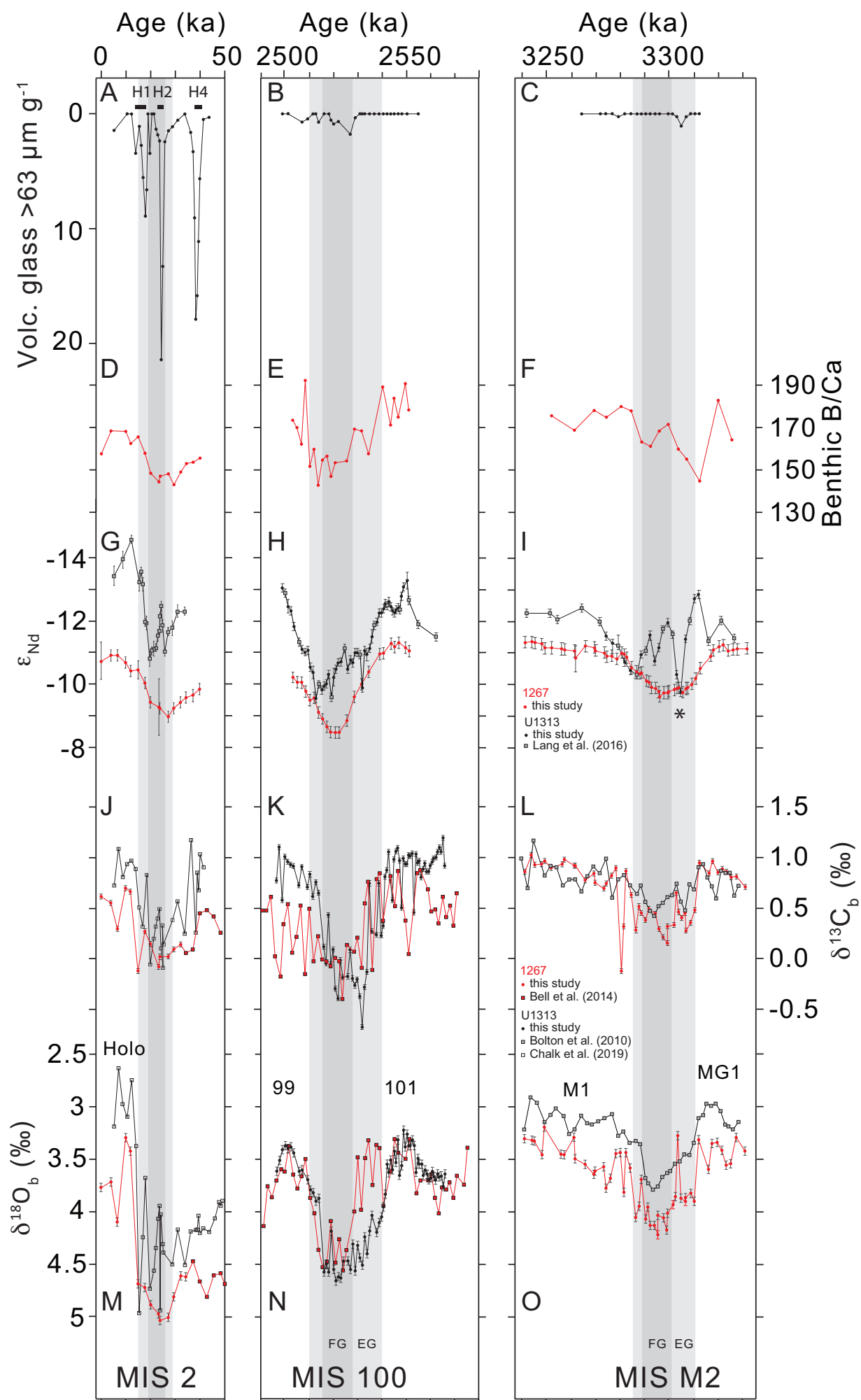
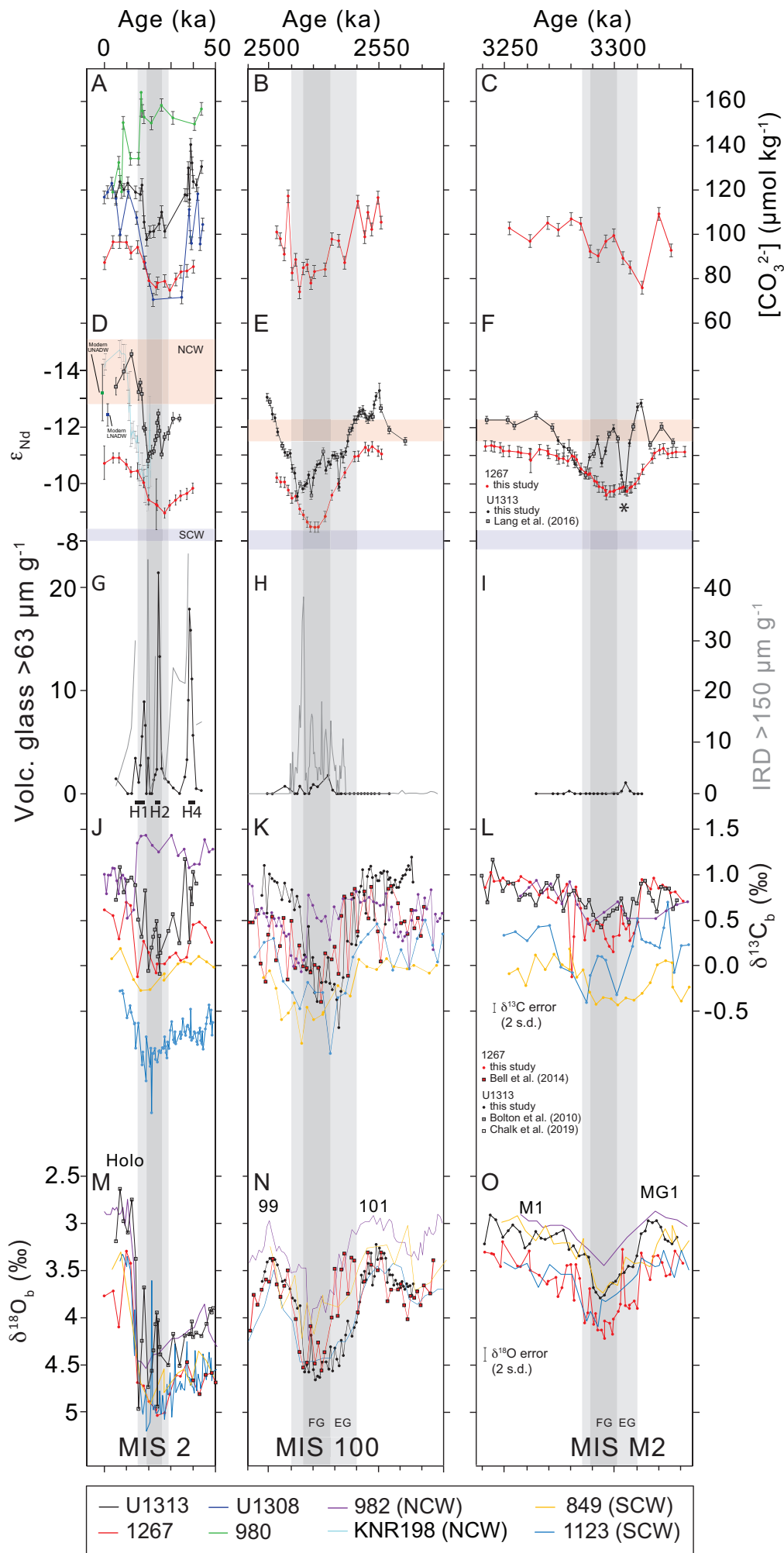Figure 1

Figure 2

Figure 3

Figure 4

Figure 5



**A**

δ¹³C (‰) — $\delta^{13}C$ (‰)

biology line

$CO_2$ influx/evasion line

Pacific

Last Glacial data key for:
U1313  1267  980  U1308
● MIS 2    ○ Holocene

Southern Ocean

T inc.
biology
Alkalinity dec.    $CO_2$ invasion
$CO_2$ influx    Alkalinity inc.
T dec.

$[CO_3^{2-}]$ (μmol kg⁻¹)

**B**

$\delta^{13}C$ (‰)

biology line

$CO_2$ influx/evasion line

Pacific

Site 1267 data key
● MIS 2      ○ Holocene
● 100        ○ 99
             ○ 101
● M2         ○ M1
             ○ MG1

Southern Ocean

T inc.
biology
Alkalinity dec.    $CO_2$ invasion
$CO_2$ influx    Alkalinity inc.
T dec.

$[CO_3^{2-}]$ (μmol kg⁻¹)

Figure 6

Age (ka)

A
CO$_2$ (ppm)
NHG threshold
(280 ppmv)

B
Insolation (w m$^2$)
June 21$^{st}$ 65˚N
December 21$^{st}$ 65˚S

C
$\varepsilon_{Nd}$
$\delta^{13}C_b$ (‰)

D
$\varepsilon_{Nd}$
SCW incursion?
$\delta^{13}C_b$ (‰)

E
[CO$_3^{2-}$] (µmol kg$^{-1}$)

F
$\delta^{18}O_b$ (‰)
M1
MG1
FG  EG
MIS M2

U1313          982 (NCW)      849 (SCW)
1267           1123 (SCW)
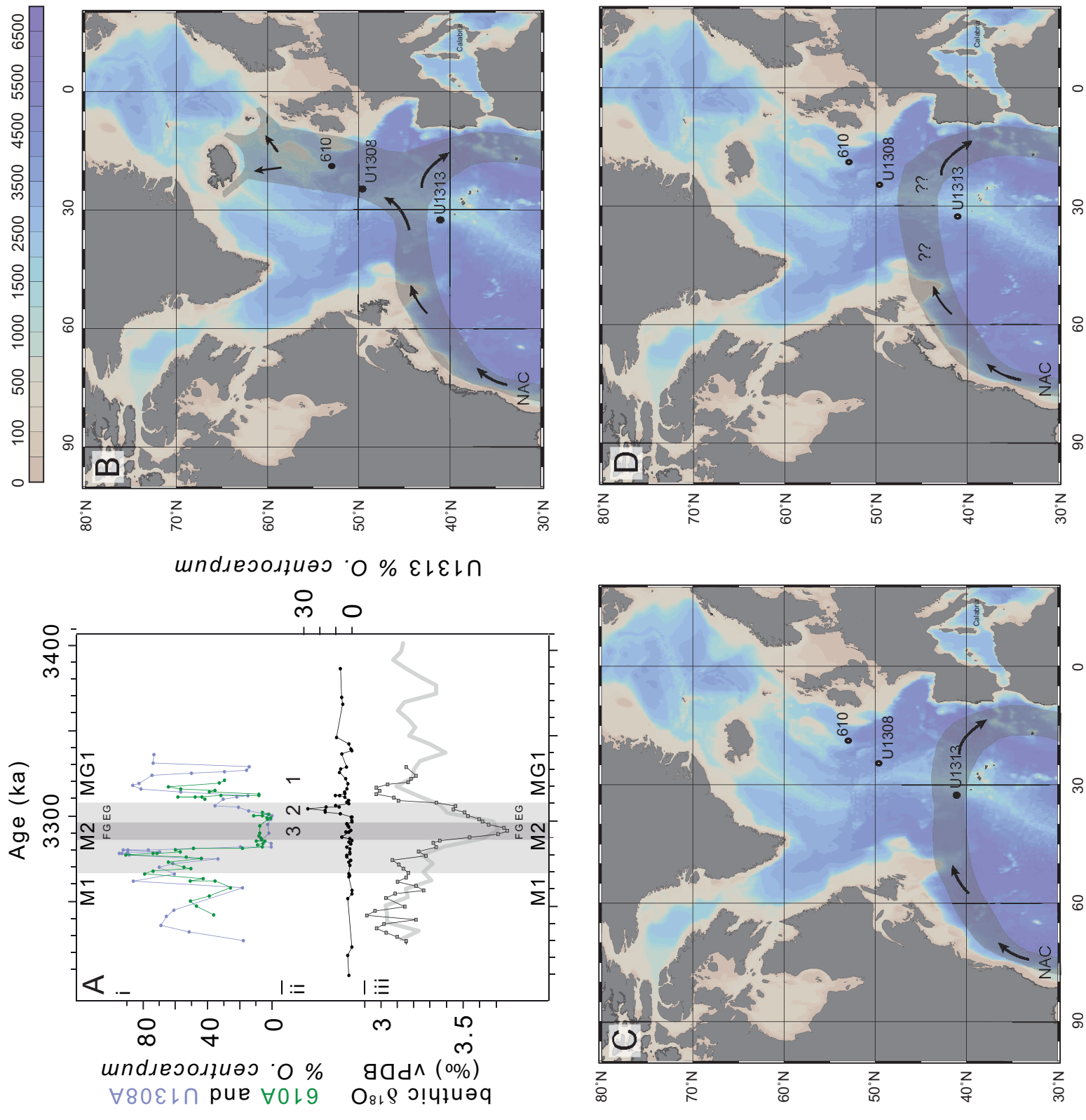
Figure 7

Figure 8

Kirby et al.: On climate and abyssal circulation in the Atlantic Ocean during late Pliocene marine isotope stage M2, ~3.3 million years ago

**Conflict of interest statement:** The authors declare that they have no competing financial interests or personal relationships that influenced the work reported in this paper

**Author Contributions:** N.K generated the Site 1267 data and contributed to manuscript writing; I.B. designed the study, supervised N.K. in data generation and wrote the manuscript; A.B generated the Site U1313 stable isotope data for MIS 100 and contributed to manuscript writing; T.B.C. supervised R.L.P in generating the Site 1267 benthic B/Ca data and contributed to the ideas presented and to manuscript writing; R.L.P generated a subset of the Site 1267 data; A.J.C. supervised N.K. and R.L.P in data generation, contributed to the ideas presented and to manuscript writing; V.E.T. supervised N.K. and R.L.P. in data generation, generated the volcanic glass count data and contributed to manuscript writing; J.A.M helped to generate the Nd isotope data; G.L.F. contributed to the ideas presented and manuscript writing; M.E.R. contributed to the ideas presented and manuscript writing; D.K. contributed samples and to the ideas presented and manuscript writing; D.B.B contributed samples and to manuscript writing; P.A.W. designed the study, supervised N.K. in data generation, co-wrote the manuscript with I.B.